Copy 214
RM L50K16

[redacted]

NACA RM L50K16

TECH LIBRARY KAFB, NM
0143760

NACA

RESEARCH MEMORANDUM

7222

WING-ON AND WING-OFF LONGITUDINAL CHARACTERISTICS OF AN AIRPLANE CONFIGURATION HAVING A THIN UNSWEPT TAPERED WING OF ASPECT RATIO 3, AS OBTAINED FROM ROCKET-PROPELLED MODELS AT MACH NUMBERS FROM 0.8 TO 1.4

By Clarence L. Gillis and A. James Vitale

Langley Aeronautical Laboratory
Langley Field, Va.

Jim RC

[redacted]

NATIONAL ADVISORY COMMITTEE
FOR AERONAUTICS
WASHINGTON
March 14, 1951

[redacted]

19.98/13

[redacted]

Classification cancelled (or changed to Unclassified)

By Authority of Nasa Tech Pub Announcement #122
(OFFICER AUTHORIZED TO CHANGE)

By ..... 3 Dec 67

NK
(GRADE OF OFFICER MAKING CHANGE)

22 Mar 61
DATE

TECH LIBRARY KAFB, NM
0143760

NATIONAL ADVISORY COMMITTEE FOR AERONAUTICS

RESEARCH MEMORANDUM

WING-ON AND WING-OFF LONGITUDINAL CHARACTERISTICS OF AN AIRPLANE CONFIGURATION HAVING A THIN UNSWEPT TAPERED WING OF ASPECT RATIO 3, AS OBTAINED FROM ROCKET-PROPELLED MODELS AT MACH NUMBERS FROM 0.8 TO 1.4

By Clarence L. Gillis and A. James Vitale

SUMMARY

Flight tests at Mach numbers from 0.8 to 1.4 were conducted on three rocket-propelled general research models of an airplane configuration. Two of the models had thin unswept tapered wings of aspect ratio 3 and hexagonal airfoil sections. The two wings had different structural stiffness characteristics. The third model had no wing. Static and dynamic longitudinal stability, control, trim, and drag characteristics were obtained. The separate effects of the various airplane components on some of the characteristics were determined. The data were obtained by analyzing the response of the models to rapid deflections of the horizontal tail.

The results obtained indicated some nonlinearity with lift coefficient of the lift-curve slope and static stability characteristics at high subsonic speeds. The variation of the lift-curve slopes with Mach number was fairly gradual. The variation with Mach number of the static stability was rather irregular, which was apparently caused by the addition of the wing to the configuration. The addition of the wing also caused the damping-in-pitch factor to vary considerably with Mach number in the transonic region. Buffeting of the models with wings was observed at high subsonic speeds at lift coefficients a little below the maximum. The drag-rise Mach number was about 0.90 for this configuration. The fuselage accounts for about one-half of the minimum drag of the configuration. The variation of drag with lift coefficient indicated that the resultant aerodynamic forces on the wing and tail were approximately normal to the chord lines.

INTRODUCTION

A general research program has been initiated by the NACA to determine by means of rocket-propelled models in free flight, the transonic and supersonic longitudinal stability, control and drag characteristics of airplane and missile configurations (references 1 to 4). The information is obtained by recording and analyzing the response of the models to intermittent disturbances in pitch applied to the models as they traverse the speed range. Presented herein are the results from the flights of two models of an airplane configuration having an unswept tapered wing of aspect ratio 3 and 4.5-percent-thick airfoil sections and of one similar model without a wing. From these results the total effects of the wing can be determined. The two models with wings were identical except that one had a solid-steel wing, whereas the other had a solid-aluminum wing. The total effects on the configuration of a change in wing flexibility thus appear in the results. Part of the data in a preliminary form and a detailed discussion of the analysis method have been presented in reference 1.

For the models discussed in this paper, all-movable horizontal tails were used for elevator control, and during the flights the horizontal tails were deflected in alternate positive and negative directions in approximate square-wave programs. The basic aerodynamic parameters defining the longitudinal stability, control effectiveness, and drag characteristics were derived from the flight time histories for a Mach number range from 0.8 to 1.4.

The models were flown at the Langley Pilotless Aircraft Research Station, Wallops Island, Va.

SYMBOLS

C_N normal-force coefficient $\left(\frac{a_n}{g}\frac{W}{qS}\right)$

C_c chord-force coefficient $\left(\frac{-a_l}{g}\frac{W}{qS}\right)$

C_L lift coefficient $(C_N \cos \alpha - C_c \sin \alpha)$

C_D drag coefficient $(C_c \cos \alpha + C_N \sin \alpha)$

$C_{D_{min}}$ minimum drag coefficient

C_m pitching-moment coefficient

a_n	normal acceleration as obtained from accelerometer, feet per second per second
a_l	longitudinal acceleration as obtained from accelerometer, feet per second per second, positive forward
g	acceleration of gravity, feet per second per second
p	free-stream static pressure, pounds per square foot
p_o	standard sea-level static pressure (2116 pounds per square foot)
V	velocity, feet per second
q	dynamic pressure $\left(\frac{\gamma}{2} pM^2\right)$
M	Mach number
γ	specific heat ratio (1.40)
R	Reynolds number, based on wing mean aerodynamic chord
S	wing area (including the area enclosed within the fuselage), square feet
S_t	horizontal tail area (including the area enclosed within the vertical tail), square feet
y	lateral distance from side of fuselage, inches
$\frac{b_e}{2}$	wing semispan measured from side of fuselage, inches
$\bar{c}$	wing mean aerodynamic chord, feet
c_t	tip chord of wing, inches
G	torsional modulus of elasticity, pounds per square inch
m_θ	wing torsional-stiffness parameter, inch-pounds per radian
m	couple applied near wing tip in plane parallel to model center line and normal to chord plane, inch-pounds
θ	local wing twist angle produced by m measured in plane parallel to that of m, radians (when used as a subscript)

θ	angle of pitch, degrees
I_y	moment of inertia about y-axis, slug-feet^2
α	angle of attack, degrees
δ	elevator deflection, degrees
ϵ	downwash angle, degrees
ϵ_o	downwash angle at zero angle of attack, degrees
P	period of pitching oscillation, seconds
t	time, seconds
$T_{1/2}$	time to damp to one-half amplitude, seconds
C_{m_o}	pitching-moment coefficient at zero angle of attack and zero elevator deflection

Subscripts:

T	trim

$$\dot{\alpha} = \frac{d\alpha}{dt}\frac{\bar{c}}{2V}$$

$$q = \frac{d\theta}{dt}\frac{\bar{c}}{2V}$$

W	wing
f	fuselage

The symbols α, $\dot{\alpha}$, δ, and q used as subscripts indicate the derivative of the quantity with respect to the subscript, for example, $C_{L_\alpha} = \frac{dC_L}{d\alpha}$.

MODELS AND APPARATUS

Models

A drawing of the complete airplane configuration investigated is shown in figure 1. The wingless model is shown in figure 2. For the wingless model, it was necessary to add a vertical tail to the bottom of the fuselage to prevent large rolling motions resulting from yaw disturbances. Photographs of the models are shown in figure 3.

The model was designed as a general research vehicle for investigating the effects on airplane stability, control effectiveness, and drag characteristics of changes in the various airplane components. The fuselage was not an optimum shape for low drag but was selected from considerations of ease of fabrication and adaptability for altering various components. The fuselage was composed of a cylindrical center portion with nose and tail sections defined by the ordinates in table I. A fairly large vertical tail was provided to insure adequate directional stability for widely different wing configurations. The following letter symbols are used throughout this paper to designate the three models:

Model designation	Description
A	Steel wing
B	Aluminum wing
C	Wingless

The wings and horizontal tails had 4.5-percent-thick hexagonal airfoil sections as shown in figure 1. Model A had a solid-steel wing (reference 1) and model B had a solid-aluminum wing. The horizontal tails were solid aluminum on all three models.

The horizontal tail was mounted on a ball bearing built into the vertical tail and was rotated about a hinge line located at 42 percent of the tail mean aerodynamic chord (fig. 4). The horizontal tail was deflected in alternate positive and negative directions during the flights by means of an electric motor and cam arrangement in models A and B and a hydraulic control system in model C. The control-position pickup was located on the lower end of the elevator push rod. The measured elevator motion can therefore be considered as the motion of the root of the elevator. As can be seen in figure 4, a gap existed between the vertical tail and the root of the horizontal tail. This

gap extended over the forward and aft 30 percent of the horizontal tail root chord. Its width was approximately 1/2 percent of the chord.

An additional noninstrumented model shown in figure 5 was flown to determine the drag of the extra vertical tail used on model C. Two scaled-down vertical tails were mounted as wings on a fin-stabilized body of revolution and flown at zero lift to determine the minimum drag. The model drag was determined from the velocity-time curve obtained by the Doppler radar. The drag of the vertical tails was obtained by subtracting the drag of the body plus fins (reference 5) from the drag of the complete model.

Instrumentation

Models A and B contained six-channel telemeters transmitting measurements of normal and longitudinal acceleration, elevator deflection, angle of attack, total pressure, and a reference static pressure. Model C had a seven-channel telemeter giving records of the same six quantities plus an additional static pressure. Angle of attack was measured by a vane-type instrument located on the nose of the model (figs. 1 to 3). This device is more fully described in reference 6. The total-pressure tube was located on a small strut below the fuselage (figs. 1 to 3). On all three models the reference static pressure measured was the pressure inside the cone of the angle-of-attack vane. Model C also had a static-pressure orifice located on the top of the fuselage at 4.9 inches behind the beginning of the cylindrical section. The total- and static-pressure locations had been calibrated previously for zero angle of attack on instrumentation test models.

Doppler radar and tracking radar units were used for obtaining checks on model velocity, range, and elevation as functions of time. Atmospheric conditions were determined from radiosondes released shortly after each flight. Fixed and manually operated 16-millimeter motion-picture cameras were used to photograph the launching and the first part of the flights.

Launching Procedure

The models were boosted to maximum velocity by a 6-inch-diameter solid-fuel Deacon rocket. The models contained no sustaining rockets. The tapered after ends of the models fitted into adaptors on the booster rockets (fig. 6). This type of attachment permitted freedom in roll and forward movement of the model with respect to the booster but restrained the model in yaw and pitch. Separation of the models from the boosters was accomplished by reason of the different drag/weight ratios of the model and booster following booster burnout. The models were launched

at angles of approximately 45° from the horizontal, by means of a crutch-type launcher as shown in figure 6.

Preflight Measurements

The measured mass characteristics of the models are given in table II. The torsional stiffness characteristics of the wings were determined by applying a couple at the tip and measuring the twist at several sections. The results are shown in figure 7. The factor plotted, Gc_t^3/m_θ, is a nondimensional parameter which makes the result independent of size or material of construction. Measured points from three other geometrically similar wings, one larger (unpublished) and two smaller (reference 7) than those described herein, are included on the curve in figure 7. For use in comparing the aeroelastic properties of these wings with other results, the values of free-stream static pressure divided by the standard sea-level pressure are shown in figure 8 for each of the three models.

TEST AND ANALYSIS PROCEDURES

Tests

The data on the characteristics of the models were obtained during the decelerating part of the flights following separation of the model and booster. The Doppler radar obtained velocity data for all three models during the boost period but failed to track the models after booster separation. The tracking radar obtained flight-path information for all models during the boost period and for model C during the entire flight. For models A and B the Mach numbers and dynamic pressures during decelerating flight were therefore determined from the telemetered total and static pressures.

The angles of attack measured by the vane on the nose of the model were corrected to angles at the model center of gravity by the method of reference 6.

The Reynolds numbers (based on the wing mean aerodynamic chord) obtained during the flights are shown in figure 9 as a function of Mach number.

The models discussed herein served as development models for evaluating and improving the testing and analysis procedures, and as such, incorporated various changes as the program proceeded. For model A, elevator deflections of approximately ±2° were used with a

programming rate of one cycle per second in an approximate square-wave pattern. This rate was too fast to permit the determination of damping or trim characteristics at the lower Mach numbers (reference 1). The elevator on model B was deflected between +4° and -2° at a rate of about one cycle in 1.7 seconds and the center of gravity was placed farther forward to give smaller oscillation periods.

During the first elevator deflection (at $M = 1.37$) following booster separation on model B the elevator moved about 1° and then stopped, probably because the hinge moments were too great for the power system. At a Mach number of about 1.17 the elevator began moving again and operated normally thereafter. Between these Mach numbers no oscillation data were obtained. At subsonic speeds the elevator did not remain at a fixed deflection for either model A or B during some of the oscillations. The elevator was overbalanced at subsonic speeds and apparently moved off the stop due to accidental play in the system as the hinge moment reversed during the oscillation. For model A the amount of elevator motion was small (0.25° or less) and its effect on the model motion was negligible. For model B the elevator motion was about 0.6° and caused an appreciable change in the character of the oscillation. These oscillations were not used in the determination of stability and damping data.

Because of the difficulties encountered on models A and B a new control system was designed for model C. This was a hydraulic system having a much greater power output than the original electric motor and cam system, and having a positive stop for the elevator. The deflection of the elevator was more nearly a step function than for the other two models and the elevator remained at a fixed deflection during all of the free oscillations. The elevator on model C was deflected between +3° and -1.2° at a rate of one cycle in 1.9 seconds.

Analysis

After each elevator deflection the models experienced short-period transient oscillations of angle of attack and normal and longitudinal accelerations. These oscillations and the subsequent steady-state values were analyzed by the method described in appendix A of reference 1 to find the longitudinal aerodynamic characteristics. The method is essentially a graphical procedure with a minimum of computational work. Its success depends to a large extent upon the accurate measurement of angle-of-attack changes of the oscillating aircraft to permit a direct determination of the lift-curve slope and the control effectiveness. The method does not require the reduction of the data to frequency-response form before the determination of the aerodynamic derivatives. If desired, the frequency-response characteristics can of course be calculated from the aerodynamic derivatives.

All of the procedures so far proposed for determining aerodynamic derivatives from free-flight tests assume that the aerodynamic coefficients are linear functions of the variables. The results shown herein and other unpublished results of rocket model tests indicate that in the transonic region this will often not be true. The nonlinearities usually appear as different slopes C_{L_α} and C_{m_α} measured when the model is oscillating over different ranges of lift coefficient. When nonlinearities appear, the slopes obtained should be considered as average values over the range of lift coefficient covered. Reference 8 contains a detailed study of the effects of nonlinear derivatives on aircraft motions. Considerable judgment is sometimes necessary in interpreting the results obtained when nonlinearities exist. For example, reference 1 lists three ways by which C_{L_δ} can be found. If the aerodynamic quantities are nonlinear, none of the methods give a true answer. However, experience with a number of rocket models shows that the method of determining C_{L_δ} which is most nearly correct depends on the configuration tested. For an airplane configuration with a fairly conventional horizontal tail the distance to the center of pressure of the lift due to control deflection can be estimated fairly accurately and the most accurate value of C_{L_δ} will probably be that obtained by dividing C_{m_δ} by this distance expressed in terms of the mean aerodynamic chord. For a missile configuration having all-movable wings near the center of gravity for control, this distance cannot be accurately estimated. For such a configuration C_{L_δ} will be of the same order of magnitude as C_{L_α} and thus equation (A-17) in reference 1 relating these quantities to $C_{L_{\delta_{trim}}}$ should give a more nearly correct result.

For determining the period and damping of the oscillations, the angle-of-attack time history is used rather than the lift coefficient. The equations show that the angle-of-attack oscillation is affected only a small amount by the lift-curve slope, whereas the lift coefficient oscillation is directly dependent on the lift-curve slope. Thus, if a nonlinear C_{L_α} exists, the period and damping obtained from the angle-of-attack oscillation are more nearly a correct measure of the static stability and damping characteristics (see reference 8). The errors involved in certain simplifying assumptions made in the analysis are examined in some detail in appendixes A and B of reference 1.

The models discussed herein were not roll-stabilized and were thus free to roll under the action of any structural asymmetry. The actual rate of roll during flight was not measured. Reference 9 shows that the steady rate of roll required to alter the longitudinal stability significantly is of the same order of magnitude as the natural frequency in pitch. For the lowest pitching frequency encountered on these models this would necessitate a rate of roll of about 3 revolutions

per second. The differential wing incidence required to produce this motion would be about 2° or greater. Since the wings were machined in one piece, the actual differential incidence should be less than 0.1°. The effects of roll on the data presented herein should therefore be negligible.

ACCURACY

It is impossible to establish the absolute accuracy of the measured quantities on any given model because the instrument calibrations can not be checked during or after the flight. The repeatability of data obtained from identical models or from identical components on different models furnishes the best check on the over-all accuracy. In general, the possible instrument errors should be proportional to a certain percentage of the total calibrated range of the instrument. Most of the probable instrumentation errors occur as errors in absolute magnitude. Incremental values or slopes and the variation with Mach number of the various quantities should in general be more accurate than the absolute values. The following table gives estimated values of the possible systematic errors in the absolute values of C_L and C_D, as affected by the accelerometer calibration ranges:

Model	M	ΔC_L	ΔC_D
A	0.80	±0.040	±0.020
B	.80	±.040	±.005
C	.80	±.014	±.005
A	1.30	±.015	±.008
B	1.30	±.015	±.002
C	1.30	±.005	±.002

The random errors may be judged by the scatter of the data points shown in the figures. Model A was the first model flown in this research program and the longitudinal accelerometer was calibrated to cover the thrust range as well as the drag range, to study the performance during the boosted phase of flight. The resulting accuracy for measuring drag was not considered satisfactory (see table above) so the longitudinal accelerometers were calibrated to cover only the drag range on models B and C.

Further errors in the aerodynamic coefficients arise because of possible dynamic-pressure inaccuracies which are approximately twice as great as the errors in Mach number. A consideration of all the factors involved indicates that the Mach numbers are probably accurate to about ±1 percent at peak velocity when Doppler radar information is obtained. The Mach numbers for all models are probably accurate to ±2 percent or

better at supersonic speeds. At subsonic speeds the Mach numbers are probably accurate to ±2 percent on models for which flight-path data are obtained by radar (model C) and are less accurate for models on which radar tracking is not obtained (models A and B). A very valuable check on the accuracy of the supersonic Mach numbers has been found to exist in the static-pressure measurements. The static-pressure sources that have been calibrated on rocket models show an abrupt pressure change at or near a Mach number of 1.0. If the Mach number at which this change occurs has been accurately determined on previous models by means of Doppler and flight-path radar, then the Mach number at this point on subsequent flights is known irrespective of errors in the pressure measurements. By using the Doppler radar at peak velocity and this pressure change at a known Mach number, the pressure measurements may be corrected for any zero shifts that may have occurred.

The errors in the measured angles of attack and elevator deflections should not vary with Mach number because they are not dependent on dynamic pressure. Probably the greatest possible error in angle of attack is caused by possible aerodynamic asymmetry of the angle-of-attack vane which is not detectable prior to flight. The elevator deflections should be accurate to about $\pm 0.1^{\circ}$ and the increments in angle of attack to about $\pm 0.2^{\circ}$.

RESULTS AND DISCUSSION

As noted in table II, the models were flown with different center-of-gravity locations, but the aerodynamic derivatives for model B presented in the figures have all been converted to values for a center-of-gravity location of 12.4 percent of the mean aerodynamic chord for comparison with models A and C. Because of the nonlinearity with lift coefficient of some of the aerodynamic derivatives at subsonic speeds, the conversion of the data to a different center of gravity may lead to some decrease in the accuracy of the results.

Lift

Figure 10 shows typical plots of the lift curves obtained for the three models. The data points shown are those reduced from the telemeter records at time intervals of 0.02 second. The data were recorded continuously and any number of points could be obtained for such a plot. The data obtained were plotted as lift coefficient against angle of attack during the first $1\frac{1}{2}$ or 2 cycles of each oscillation.

The data for model C in figure 10 are plotted to the same scale as the data for models A and B. As pointed out in the section "ACCURACY,"

however, the lift coefficients for model C are considerably more accurate than for the other two models because of the more sensitive accelerometer. In the process of finding lift-curve slopes the curves for model C were plotted to a much larger scale commensurate with their accuracy. Two curves are faired through each set of data illustrated for model C in figure 10, one curve connecting points measured while the angle of attack was increasing and one curve for points obtained while the angle of attack was decreasing. The difference is in such a direction as to appear as a phase lead of the lift coefficient ahead of the angle of attack, which is in the opposite direction to what might be expected from potential-flow unsteady-lift considerations (reference 10). The same effect, of approximately the same magnitude, can be detected in some of the curves for models A and B when plotted to the larger scale used in the data analysis. In some cases the scatter of the data points for models A and B, attributable to the less sensitive accelerometers, masks the difference caused by the direction of angle-of-attack change. On models A and B the effect is much larger at subsonic speeds than at supersonic speeds and is larger at high lift coefficients than at low lift coefficients.

Part of the difference in lift at a given angle of attack can be accounted for by the lift derivatives $C_{L_{\dot{\alpha}}}$ and C_{L_q}. The calculated effect from estimated values of $C_{L_{\dot{\alpha}}}$ and C_{L_q} is shown for several curves in figure 10. The largest difference in lift at a given angle of attack occurs for model A at the points where the airfoil appears to have stalled. The same effect on stalled airfoils is observed in static wind-tunnel testing. The lift data in reference 4 show the same effect of rate of angle-of-attack change on the lift, but the effect is greater in reference 4 than for the models described herein. The model in reference 4 also had a wing with hexagonal airfoil sections, the rear wedge of the airfoil being more blunt than those on the models herein. Reference 3, presenting data for a model with a circular-arc airfoil, showed only a very small effect of rate of change of angle of attack. The possibility exists that the effect under discussion is caused by asymmetric air-flow separation even at low lift coefficients and is a function of the type of airfoil section.

The lift-curve slopes obtained for the three models are shown in figure 11. Some additional points from small-amplitude oscillations are shown for model A which were not included in the preliminary analysis of reference 1. Slopes measured from motions of small amplitude could be expected to be less accurate than those from larger amplitude motions.

No large or abrupt changes in lift-curve slope with Mach number occur in the transonic region. This behavior is probably attributable to the low aspect ratio and the thin airfoil sections of the wing and horizontal tail. Thicker airfoil sections or higher aspect ratios have been shown

to cause larger variation in lift-curve slope at high subsonic speeds (reference 11).

The data from all three models show some nonlinearity of the lift curves with angle of attack in the transonic region. The relative magnitude of the nonlinearity is greater for the wingless model, probably because of the greater proportionate effect of the fuselage.

Differences occurred between the slopes measured for the two winged models (fig. 11(a)), model B having higher slopes up to $M = 1.15$ and lower slopes at $M = 1.4$. A calculation of the effect of wing twist at a Mach number of 0.8, using the stiffness curve in figure 7, showed a possible difference in C_{L_α} of 2 percent which is within the accuracy of measuring the slopes. The increase in dynamic pressure with Mach number and a movement of the wing aerodynamic center from a position forward of the elastic axis to one aft would account for the differences in lift-curve slope shown.

Figure 12 shows the lift-curve slopes of the tail and of the wing plus interference near zero lift. The values for wing plus interference were obtained by subtracting the slopes for model C from those for model A. The rocket model data for the wing lift-curve slope also include a negative increment in slope caused by the wing downwash acting on the tail. The wing-alone slopes would therefore be somewhat higher than those shown in figure 12. Also shown are values of lift-curve slope of the wing alone from unpublished tests on the transonic bump in the Southern California Cooperative Wind Tunnel of a similar wing and theoretical results at supersonic speeds for a straight rectangular wing having an aspect ratio of 3.0 (reference 12). The wind-tunnel and rocket model data show similar variations with Mach number. The agreement between the rocket model results and the theoretical calculations is relatively good. Since the lift added by the wing on the rocket model is as great or greater than that for the wing alone as tested in the wind tunnel, the indications are that the wing area included in the fuselage (about 27.5 percent) may be considered almost fully effective in producing lift on this configuration. Since the wing and horizontal tail are identical in plan form and airfoil section, the lift effectiveness of the tail (fig. 13) should equal the lift-curve slope of the wing alone when multiplied by the area ratio of the two surfaces. Such a curve $\left(\frac{\Delta C_L}{\Delta\delta}\frac{S}{S_t}\right)$ is shown in figure 12. The smaller slopes shown for the tail are probably caused by the gaps at the root of the tail.

The values of $\Delta C_L/\Delta\delta$ in figure 13 are in good agreement for the three models. Because the tail lift was a much greater proportion of the total lift for model C, the values of $\Delta C_L/\Delta\delta$ are more accurate for this model than for the other two models. The tail lift-curve slopes should also be nonlinear with lift coefficient but the method of

determining $\Delta C_L/\Delta\delta$ does not permit the determination of this effect and the data are thus shown as incremental values rather than slopes.

If it is assumed that the $d\epsilon/d\alpha$ acting on the tail of the wingless model is negligible, then the difference between the lift-curve slope C_{L_α} for model C and the $\Delta C_L/\Delta\delta$ for model C will give the lift-curve slope of the fuselage. The nonlinearity of the curves of C_{L_α} prevents this procedure from being used, but at the lowest and highest Mach numbers attained the indications are that the fuselage slope is of the order of 0.002 or 0.003, which approaches the accuracy of measuring the slopes on this model.

Maximum Lift and Buffeting

The data on models A and B indicated that maximum lift coefficients and some buffeting information were obtained over a range of high subsonic speeds. A discussion of the maximum lift coefficients is given in reference 1 and the buffeting information is discussed in some detail in reference 13. Figure 14 is a summary of the information obtained showing the maximum lift coefficients and the region where buffeting was observed. A curve is also shown defining the highest lift coefficients reached. At these values the maximum lift coefficient of the configuration has not yet been reached. Below this curve and outside the cross-hatched area no evidence of buffeting appeared in the records.

Drag

Minimum drag coefficients for all three models are shown in figure 15. The data for model A, from reference 1, have been omitted below a Mach number of 1.07 because they are inaccurate at subsonic speeds as indicated by a comparison of the measured minimum drag coefficients for model A with those for models B and C, which had considerably more sensitive longitudinal accelerometers. At Mach numbers above 1.0 the accuracy is much better and the agreement between models A and B was good.

The drag divergence Mach number for this configuration is apparently about 0.90. A breakdown of the minimum drag coefficient into its various components is shown in figure 16, all coefficients being based on total wing area. The drag of the vertical tail was determined from the special model flown for this purpose. The drag for fuselage-plus-tail surfaces was obtained by subtracting the drag of one vertical tail from the drag of model C. This drag subtracted from that for models A and B gives the drag of the wing. Multiplying the minimum drag of the wing by the ratio of exposed horizontal tail area to exposed wing area

gives the drag of the horizontal tail. The drag of the fuselage was found by subtracting the drag of two vertical tails and one horizontal tail from the drag of model C. The drag values obtained as described of course include some unknown interference effects. The fuselage drag is seen to be about one-half of the minimum drag of the airplane at all Mach numbers. When this drag is compared with that of the parabolic bodies tested in reference 14, it is evident that the fuselage drag is fairly high when based on maximum cross-sectional area but is not unreasonable when based on the fuselage volume.

The minimum drag coefficients of the wing and horizontal tail can not be considered as very accurate when obtained in the manner described. For comparison, the wing drag, obtained from the data of reference 7 and unpublished body drag data, is shown in figure 16. The wings on the models in reference 7 were similar to those on models A and B, but they had deflected ailerons and were rolling continuously. The wing minimum drag coefficient, obtained as described herein, appears to be of the right order of magnitude and is only a small part of the minimum drag of the configuration.

The variation of drag with lift is shown in figure 17 in the form of dC_D/dC_L^2. Although the minimum drag for model A was inaccurate at subsonic speeds, it appears that the factor dC_D/dC_L^2 is of the right order of magnitude when compared with model B although the scatter of the data points is greater than for model B. This is in accord with the statements in the section on "ACCURACY" that most of the errors in telemetered quantities occur as drifts in the zero value rather than changes in slope. Comparison of the values of dC_D/dC_L^2 shown for models A and B with the factor $1/57.3C_{L_\alpha}$ for both models indicates that the resultant force is approximately normal to the wing chord. Comparison of the values of dC_D/dC_L^2 for model A at $M = 1.35$ with those for model B indicates that the values for model A are somewhat larger. The reason for this difference is not definitely known but the values for model A were obtained from oscillations of larger amplitude and the possibility of some nonlinearity of dC_D/dC_L^2 with lift coefficient exists.

Values of maximum lift-drag ratio and of C_L at which maximum lift-drag ratio occurs are shown in figures 18 and 19. The symbols designate points where the maximum values were actually measured. At other Mach numbers the values represented by the faired curve were obtained by an extrapolation of the drag curves based on the measured values of $C_{D_{min}}$ and dC_D/dC_L^2. The relatively low values of $(L/D)_{max}$

and high values of C_L for $(L/D)_{max}$ are both a reflection of the high drag of the fuselage.

Static Stability

The measured periods of oscillation of the angle of attack are shown in figure 20. Not many points are available for model B because of the difficulties encountered with the control system as mentioned previously. The data converted to C_{m_α} for a center of gravity at 12.4 percent of the mean aerodynamic chord are shown in figure 21. Above a Mach number of 1.0 some difference existed between models A and B, with model B exhibiting the greater stability. Further comments on this point will be made subsequently in the discussion of the trim characteristics. Model A indicated that C_{m_α} for the complete airplane varies with lift coefficient below $M = 0.92$. The wingless model showed nonlinearity at Mach numbers above 0.86.

Both models A and B showed the same type of variation of C_{m_α} with Mach number in the region where data were obtained for both models. The somewhat irregular variation with Mach number of the C_{m_α} for models A and B is apparently an effect of the wing on the configuration because C_{m_α} for model C varies smoothly with Mach number. Subtracting the values of C_{m_α} for the winged and wingless models gives the total effect of the wing on the stability of the airplane. The result is shown in figure 22 for the more rigid wing. For the center-of-gravity position used the contribution of the wing itself to $\Delta C_{m_{\alpha_w}}$ should be negative and the increment of $\Delta C_{m_{\alpha_w}}$ caused by the wing downwash on the tail will be positive. It is not possible to tell from the data what the relative magnitudes of the two effects are. It is estimated that the $\Delta C_{m_{\alpha_w}}$ due to the wing alone would be about -0.01 at subsonic speeds and about -0.02 at supersonic speeds.

By subtracting the $\Delta C_m/\Delta\delta$ of the horizontal tail from the C_{m_α} of the wingless model the stability contribution of the fuselage $\Delta C_{m_{\alpha_f}}$ is obtained. The result is shown in figure 22. This procedure assumes that the downwash over the tail due to the fuselage does not change with angle of attack. Because of the high tail position, this is probably a fairly good approximation. The value of $\Delta C_{m_{\alpha_f}}$ calculated from reference 15 is 0.017 which shows good agreement with the measured values.

The aerodynamic-center locations for the winged models A and B are shown in figure 23. Both models show the same trends with Mach number in the region where data were obtained for both models. The aerodynamic center for model B was farther rearward than for model A at Mach numbers above 1.0. The large values of dynamic pressure occurring during the tests probably exaggerate the effects of wing flexibility compared to the probable operating conditions for a full-size airplane at the same Mach number.

The aerodynamic center for the wingless configuration varies around an average position at about 200 percent of the mean aerodynamic chord or about 70 percent of the fuselage length from the nose. The fuselage instability causes an average forward shift in aerodynamic center of about 18 percent of the mean aerodynamic chord on the complete configuration.

Damping in Pitch

The time required for the oscillations to damp to one-half amplitude is shown in figure 24(a) and the data converted to the damping factor $C_{m_q} + C_{m_{\dot{\alpha}}}$ and corrected to a center of gravity at 12.4 percent of the mean aerodynamic chord for model B are shown in figure 24(b). The wingless configuration shows a damping factor that is nearly constant with Mach number and exhibits some nonlinearity with lift coefficient at subsonic speed. The winged configurations have damping factors that are of roughly the same order of magnitude as those for the wingless configuration but show considerable variation with Mach number, particularly between $M = 0.90$ and $M = 1.05$. Although the damping factors $C_{m_q} + C_{m_{\dot{\alpha}}}$ are approximately equal for the winged and wingless models, the actual damping of the oscillations is considerably better for the winged models (fig. 24(a)) because of the influence of the lift-curve slope on the damping. This effect would occur on full-scale airplanes, the relative effect of the lift-curve slope depending on the radius of gyration (see reference 1).

Theoretical calculations of the damping of rectangular wings at supersonic speeds are available in reference 12. The damping derivatives C_{m_q} and $C_{m_{\dot{\alpha}}}$ were calculated for the wing alone and tail alone at Mach numbers of 1.25 and 1.40 by use of this reference. For the wing and tail combination on models A and B the increments in the derivatives due to the effect of the wing on the tail were added to the wing-alone and tail-alone derivatives. A large negative increment in $C_{m_{\dot{\alpha}}}$ occurs because of the downwash lag effect and a small positive increment in C_{m_q} exists because of the downwash angle at the tail caused by the

wing lift derivative C_{L_q}. For both calculations a value of $\frac{d\epsilon}{d\alpha} = 0.40$ was assumed. The calculations indicated that at $M = 1.25$ the $C_{m_{\dot{\alpha}}}$ of the wing alone was positive and larger than the negative C_{m_q} of the wing, resulting in a dynamically unstable wing at $M = 1.25$ for the center of gravity of the tests. When the tail was placed behind the wing the negative $C_{m_{\dot{\alpha}}}$ caused by the downwash lag overcompensated for the positive contributions of the tail alone and wing alone to $C_{m_{\dot{\alpha}}}$, resulting in a negative $C_{m_{\dot{\alpha}}}$ for the complete configuration.

The calculations also showed that the $C_{m_{\dot{\alpha}}}$ of the tail alone was small compared to the C_{m_q} of the tail. The measured damping factor $C_{m_q} + C_{m_{\dot{\alpha}}}$ for model C is therefore essentially the C_{m_q} of the tail, which is the largest contribution to the pitch damping factor and which, according to figure 24(b), does not vary much with Mach number in the range covered by the tests. Since the measured lift-curve slopes of the tail are less than the theoretical, it might be expected that the measured damping would be less than the theoretical. Figure 24(b) indicates this to be the case for models A and B, but not for model C. The measured values for all the models of course include the damping contribution of the fuselage which is not included in the theoretical calculations.

The work in reference 12 indicates that the positive values of $C_{m_{\dot{\alpha}}}$ for the wing alone and tail alone increase with decreasing Mach number at supersonic speeds. Also, the variations in static stability in the transonic region, figure 21, indicate that large changes in downwash are probably occurring. Thus it is probable that the variations with Mach number of the factor $C_{m_q} + C_{m_{\dot{\alpha}}}$ for the winged configurations are caused by the $C_{m_{\dot{\alpha}}}$ term which could become positive under conditions of small downwash.

The differences in $C_{m_q} + C_{m_{\dot{\alpha}}}$ between models A and B are not necessarily attributable to wing flexibility but are more probably a measure of the experimental accuracy of determining the damping derivatives. The primary reason is that for rocket models similar to those under consideration the contribution of the C_{L_α} term to the damping is very large and the factor $C_{m_q} + C_{m_{\dot{\alpha}}}$ is the difference between two large quantities. Small errors in C_{L_α} or in $T_{1/2}$ can therefore have a large effect on the values of $C_{m_q} + C_{m_{\dot{\alpha}}}$. For models A and B the C_{L_α} term accounted for about two-thirds of the total damping, while for model C it accounted for about one-third. Thus, the damping derivatives for model C are probably numerically more accurate than for models A and B.

Longitudinal Trim and Control Effectiveness

The trim lift coefficients and angles of attack are shown in figure 25. The trim lift coefficients for model C are not shown because they are very small (about ±0.03) compared to those for models A and B and have no great significance. The complete configuration (models A and B) does not appear to have any large trim changes in the transonic region. Model C indicated a more or less abrupt trim change in both lift coefficient and angle of attack between $M = 0.90$ and $M = 1.0$. This same type of change may or may not have occurred for the complete configuration; the number of trim points obtained in this region was not sufficient to establish definitely the correct fairing of the curves.

It would be expected that the curves of C_{L_T} and α_T for $\delta = 2.0^\circ$ would coincide for models A and B in the Mach number region where data were obtained for both models. The curve for $\delta = 2.0^\circ$ for model B was obtained by a linear interpolation from the measured values for $\delta = -2.0^\circ$ and 4.0°. The failure of the curves for models A and B to coincide may be due to an error in measuring the elevator deflection for either or both of the models or may be an indication of some nonlinearity in the variation of α_T and C_{L_T} with elevator deflection.

Both the α_T and C_{L_T} curves for model B indicate smaller increments due to elevator deflection $\left(\Delta\alpha_T/\Delta\delta \text{ and } \Delta C_{L_T}/\Delta\delta\right)$ than for model A in the region near a Mach number of 1.1 where the trim data for the two models overlap. Since the $\Delta\alpha_T/\Delta\delta$ is equal to $C_{m_\delta}/C_{m_\alpha}$ and the tail surfaces were identical on the two models, the disagreement between the two models is an indication of greater stability on model B. This agrees with the aerodynamic-center data in figure 23. Since the two indications of stability were obtained independently of each other in the reduction of the data, it appears that the greater stability on model B at $M = 1.1$ actually existed and is not the result of errors incurred in the data analysis.

The pitching-moment effectiveness of the elevator is shown in figure 26. The all-movable tail provided an effectiveness which is practically constant with Mach number. It is probable that the $dC_m/d\delta$ of the elevator is nonlinear with elevator lift coefficient or deflection, but this could not be determined from the results because only two elevator deflections were used on each model. The values shown in figure 26 are thus shown as incremental values $\Delta C_m/\Delta\delta$ and represent average values over the elevator deflection range covered by the tests. For this reason, agreement of the data for the three models is considered good.

Figure 27 presents the effectiveness of the elevator in changing the trim lift coefficient of the airplane. Since $\Delta C_m/\Delta\delta$ remains fairly constant with Mach number the decrease in $\Delta C_{L_T}/\Delta\delta$ with increasing Mach number is caused by the increase in static stability. The difference between the curves for the two models near $M = 1.1$ again indicates the greater stability of model B.

The pitching-moment coefficients at zero angle of attack and zero elevator deflection are shown in figure 28. The magnitude of C_{m_0} is about the same for the winged and wingless models, which indicates that the C_{m_0} is primarily due to the fuselage-tail combination. The converging rear portion of the fuselage (fig. 1) would cause a downflow over the tail and the drag of the horizontal and vertical tail surfaces would cause a positive pitching moment. From the drag data in figure 16 this latter effect is calculated to be $C_{m_0} = 0.010$ at $M = 1.15$ and $C_{m_0} = 0.006$ at $M = 0.85$, which are small compared to the values shown in figure 28. Since the wing and fuselage are symmetrical about the longitudinal axis the lift and thus the downwash due to lift should be zero at zero angle of attack. The elevator deflection required to trim the model at zero angle of attack should therefore be equal to the downwash at the tail which is producing the major part of the C_{m_0}. These values of downwash angle are shown in figure 29. Apparently this downwash angle is caused almost entirely by the fuselage, the angle being approximately 1° at subsonic speeds and 2° at supersonic speeds. The different variations with Mach number of the C_{m_0} and ϵ_0 curves for models B and C in the region between $M = 0.90$ and $M = 1.00$ is not necessarily attributable to the wing. As stated previously, the trim data for model B (from which C_{m_0} and ϵ_0 are determined) were not complete enough in this Mach number region to establish the correct fairing of the curves. Since the C_{m_0} and ϵ_0 are apparently caused mainly by the fuselage shape, it is probable that a variation with Mach number such as that shown for model C between $M = 0.90$ and $M = 1.00$ would be obtained for the complete configuration if more trim data were available.

CONCLUSIONS

Flight tests of rocket-propelled models (with and without wings) of an airplane configuration having thin unswept tapered wings and horizontal tails of aspect ratio 3 indicated the following conclusions:

1. The variation of lift coefficient with angle of attack was nonlinear in the transonic region. The variation of the lift-curve slopes with Mach number was fairly small and gradual.

2. The portion of the wing area enclosed within the fuselage may be considered fully effective in producing lift on this configuration.

3. An apparent reduction in lift effectiveness of the all-movable horizontal tail as compared to that of the wing occurred throughout the speed range; this reduction was probably caused by chordwise gaps at the root.

4. Buffeting of the model occurred at high subsonic speeds at lift coefficients a little below the maximum lift coefficient.

5. The minimum drag of the fuselage was about half of the drag of this configuration. The drag-rise Mach number was about 0.90 for the configuration. The minimum drag of the wing was only a small part of the minimum drag of the complete configuration.

6. The variation of drag with lift coefficient indicated that the resultant aerodynamic forces on the wing and tail were approximately normal to the chord lines.

7. The static stability of the complete configuration varied with lift coefficient at subsonic speeds. The somewhat irregular variation of static stability with Mach number is apparently an effect of the wing on the configuration.

8. The damping factor for the wingless configuration was practically invariant with Mach number. Addition of the wing caused the damping factor to have rather large variations with Mach number in the transonic region.

9. The converging rear portion of the fuselage caused a downflow over the tail which became greater as the Mach number increased.

Langley Aeronautical Laboratory
National Advisory Committee for Aeronautics
Langley Field, Va.

REFERENCES

1. Gillis, Clarence L., Peck, Robert F., and Vitale, A. James: Preliminary Results from a Free-Flight Investigation at Transonic and Supersonic Speeds of the Longitudinal Stability and Control Characteristics of an Airplane Configuration with a Thin Straight Wing of Aspect Ratio 3. NACA RM L9K25a, 1950.

2. Mitcham, Grady L., Stevens, Joseph E., and Norris, Harry P.: Aerodynamic Characteristics and Flying Qualities of a Tailless Triangular-Wing Airplane Configuration As Obtained from Flights of Rocket-Propelled Models at Transonic and Low Supersonic Speeds. NACA RM L9L07, 1950.

3. D'Aiutolo, Charles T., and Mason, Homer P.: Preliminary Results of the Flight Investigation between Mach Numbers of 0.80 and 1.36 of a Rocket-Powered Model of a Supersonic Airplane Configuration Having a Tapered Wing with Circular-Arc Sections and 40° Sweepback. NACA RM L50H29a, 1950.

4. Niewald, Roy J., and Moul, Martin T.: The Longitudinal Stability, Control Effectiveness, and Control Hinge-Moment Characteristics Obtained from a Flight Investigation of a Canard Missile Configuration at Transonic and Supersonic Speeds. NACA RM L50I27, 1950.

5. Morrow, John D., and Katz, Ellis: Flight Investigation at Mach Numbers from 0.6 to 1.7 to Determine Drag and Base Pressures on a Blunt-Trailing-Edge Airfoil and Drag of Diamond and Circular-Arc Airfoils at Zero Lift. NACA RM L50E19a, 1950.

6. Mitchell, Jesse L., and Peck, Robert F.: An NACA Vane-Type Angle-of-Attack Indicator for Use at Subsonic and Supersonic Speeds. NACA RM L9F28a, 1949.

7. Sandahl, Carl A., and Strass, H. Kurt: Rolling Effectiveness of a Thin Tapered Wing Having Partial-Span Ailerons As Determined by Rocket-Powered Test Vehicles. NACA RM L50D17, 1950.

8. Curfman, Howard J., Jr.: Theoretical and Analog Studies of the Effects of Nonlinear Stability Derivatives on the Longitudinal Motions of an Aircraft in Response to Step Control Deflections and to the Influence of Proportional Automatic Control. NACA RM L50L11, 1950.

9. Phillips, William H.: Effect of Steady Rolling on Longitudinal and Directional Stability. NACA TN 1627, 1948.

10. Statler, I. C.: Dynamic Stability at High Speeds from Unsteady Flow Theory. Jour. Aero. Sci., vol. 17, no. 4, April 1950, pp. 232-242, 255.

11. Luoma, Arvo A., and Wright, John B.: Longitudinal Stability and Control Characteristics at High-Subsonic Speeds of Two Models of a Transonic Research Airplane with Wings and Horizontal Tails of Aspect Ratios 4.2 and 2. NACA RM L50H07, 1950.

12. Harmon, Sidney M.: Stability Derivatives at Supersonic Speeds of Thin Rectangular Wings with Diagonals Ahead of Tip Mach Lines. NACA Rep. 925, 1949.

13. Gillis, Clarence L.: Buffeting Information Obtained from Rocket-Propelled Airplane Models Having Thin Unswept Wings. NACA RM L50H22a, 1950.

14. Hart, Roger G., and Katz, Ellis R.: Flight Investigations at High-Subsonic, Transonic, and Supersonic Speeds to Determine Zero-Lift Drag of Fin-Stabilized Bodies of Revolution Having Fineness Ratios of 12.5, 8.91, and 6.04 and Varying Positions of Maximum Diameter. NACA RM L9I30, 1949.

15. Munk, Max M.: The Aerodynamic Forces on Airship Hulls. NACA Rep. 184, 1924.

TABLE I

FUSELAGE NOSE AND TAIL ORDINATES

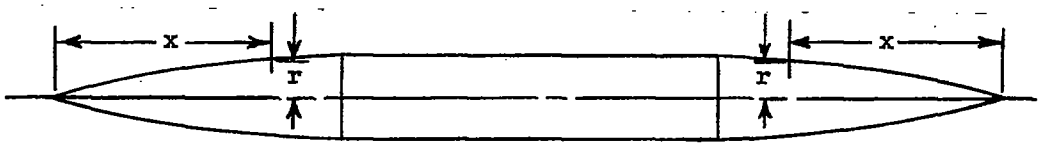

x (in.)	r (in.)
0	0.168
0.060	.182
.122	.210
.245	.224
.480	.294
.735	.350
1.225	.462
2.000	.639
2.450	.735
4.800	1.245
7.350	1.721
8.000	1.849
9.800	2.155
12.250	2.505
13.125	2.608
14.375	2.747
14.700	2.785
17.150	3.010
19.600	3.220
22.050	3.385
24.500	3.500

TABLE II

MODEL MASS CHARACTERISTICS

Model	Weight (lb)	Iy (slug ft^2)	Center-of-gravity location (percent M.A.C.)
A	126.0	8.91	12.4
B	107.0	10.87	4.6
C	88.8	10.03	12.3

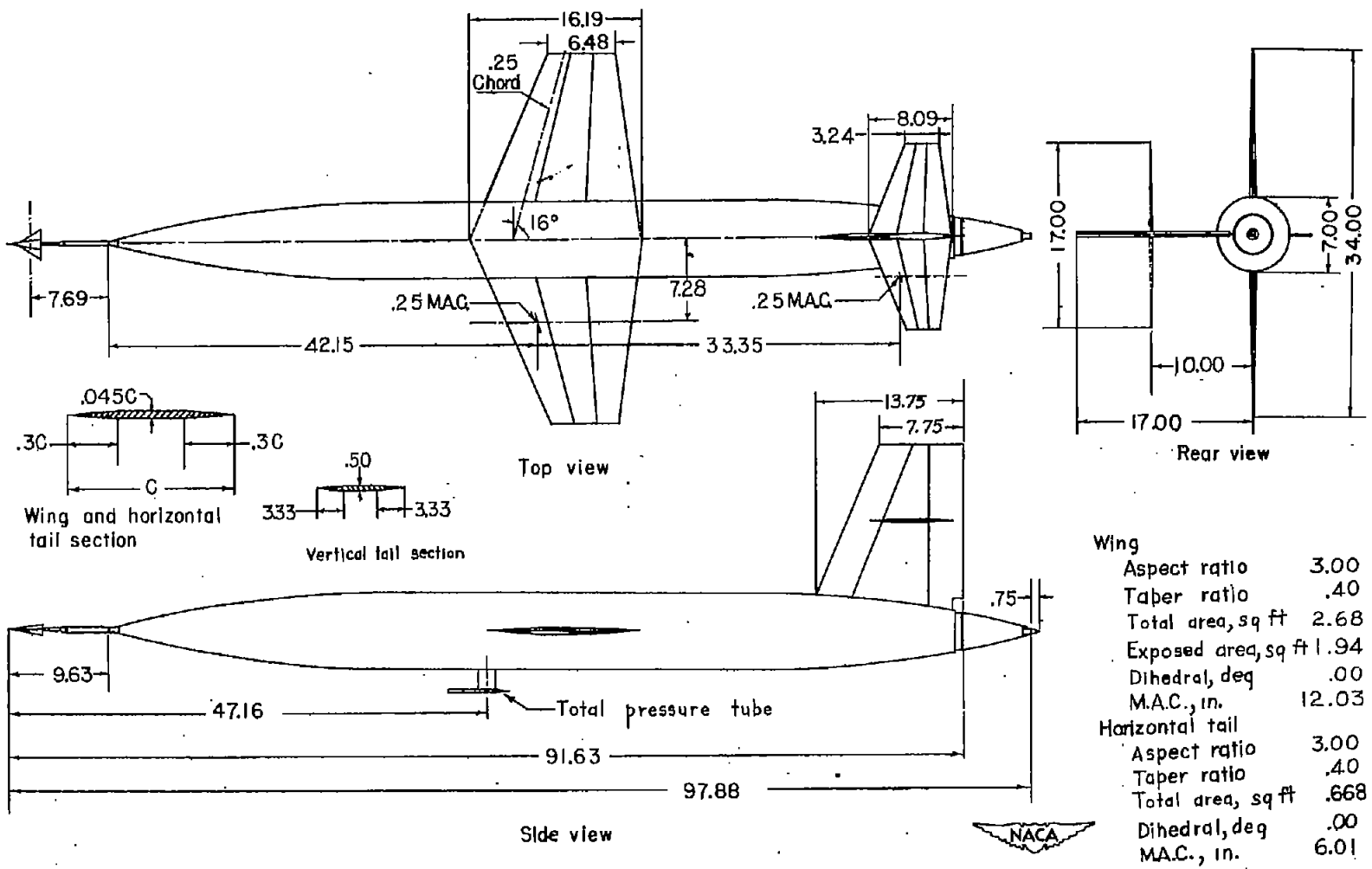

Wing	
Aspect ratio	3.00
Taper ratio	.40
Total area, sq ft	2.68
Exposed area, sq ft	1.94
Dihedral, deg	.00
M.A.C., in.	12.03
Horizontal tail	
Aspect ratio	3.00
Taper ratio	.40
Total area, sq ft	.668
Dihedral, deg	.00
M.A.C., in.	6.01
Vertical tail	
Exposed area, sq ft	1.11

Figure 1.- General arrangement of models A and B. (All dimensions are in inches.)

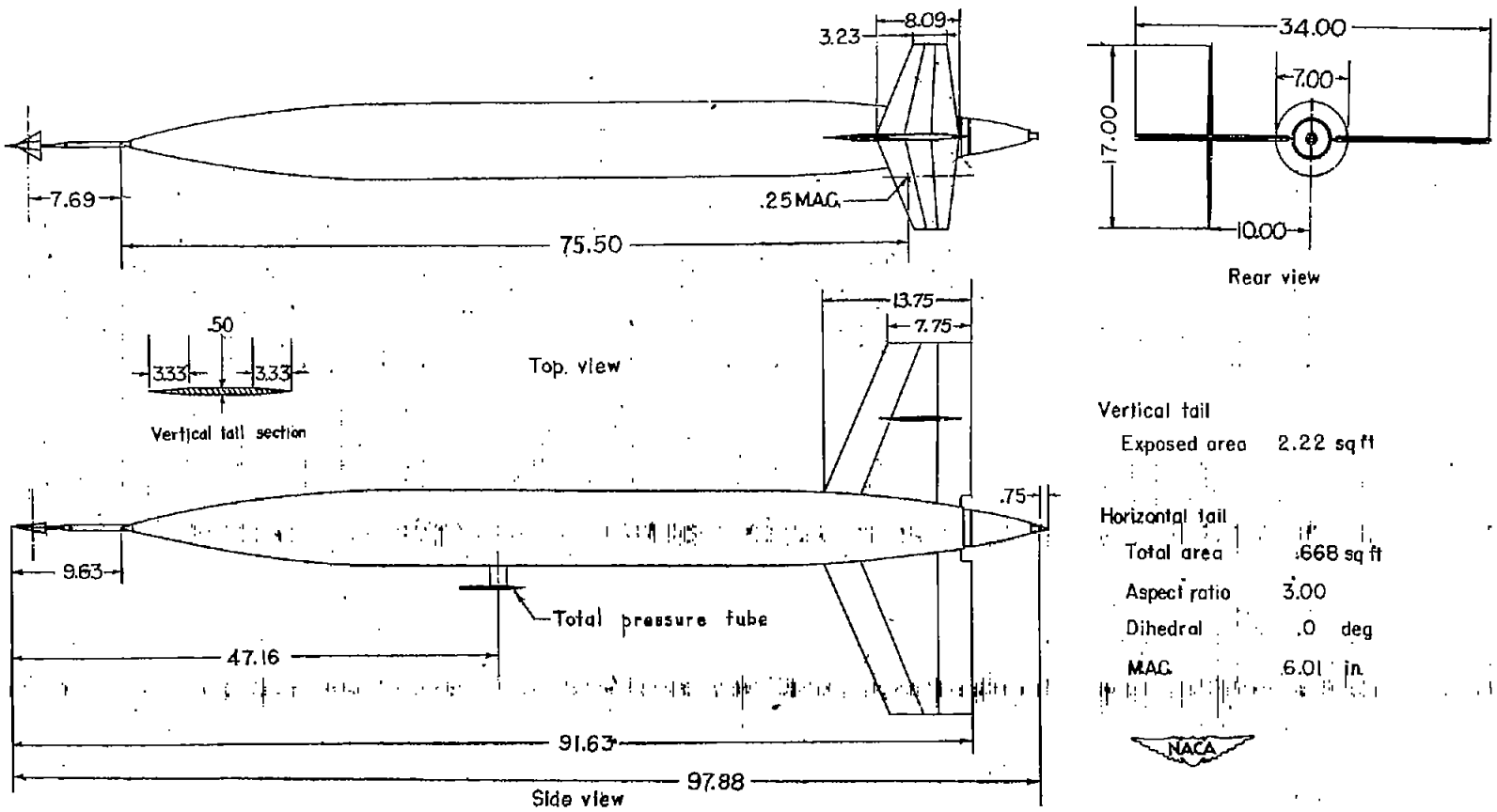

Figure 2.- General arrangement of model C. (All dimensions are in inches.)

NACA

L-59511

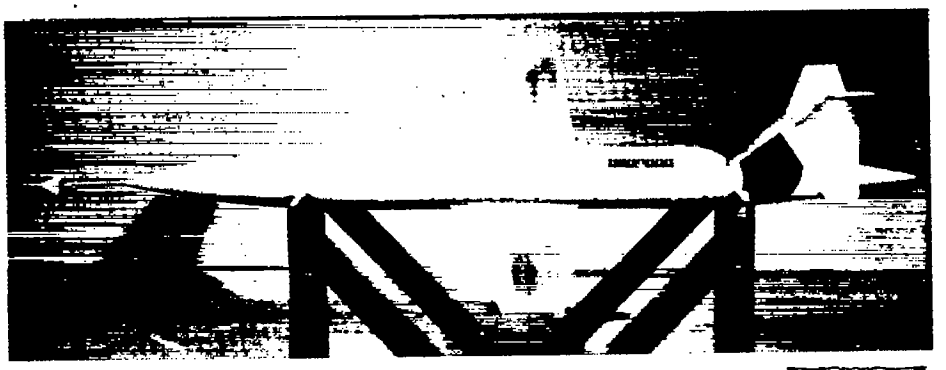

NACA

L-59512

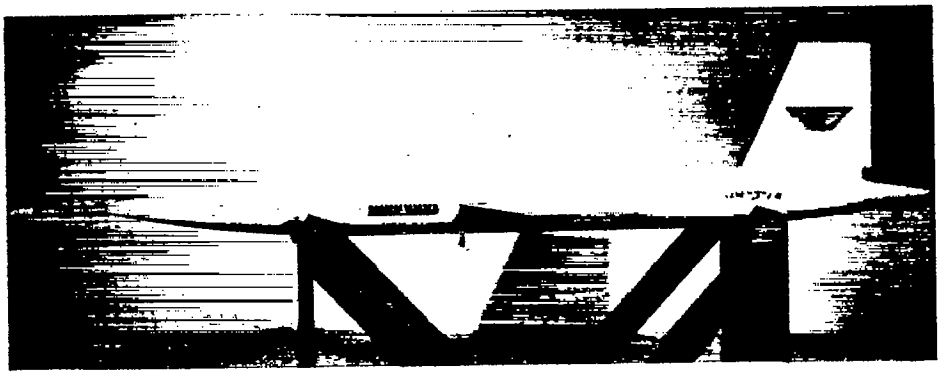

NACA

L-59513

(a) Model A.

Figure 3.- Models tested.

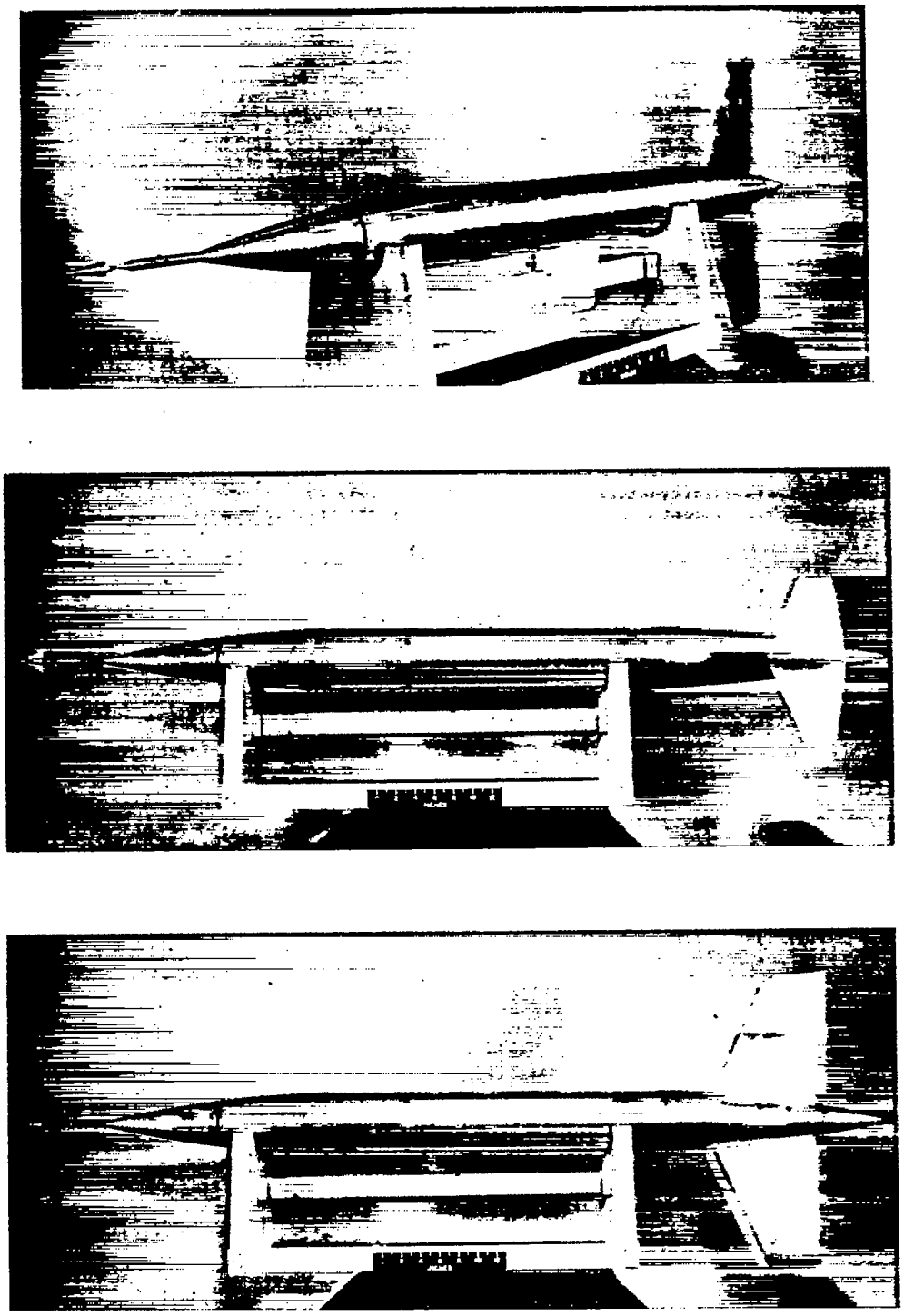

(b) Model C.

Figure 3.- Concluded.

L-64966

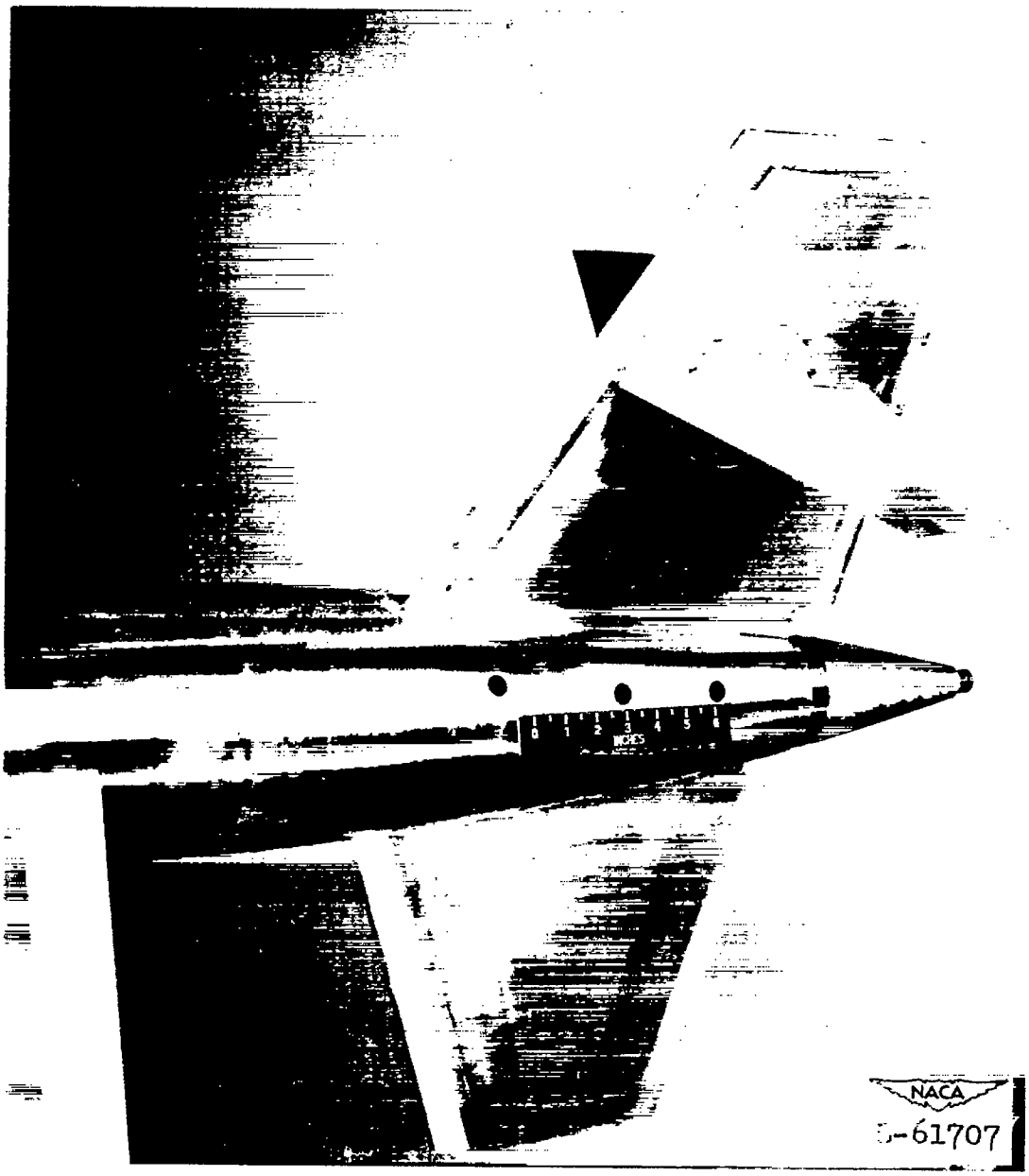

Figure 4.- Tail surfaces, model C.

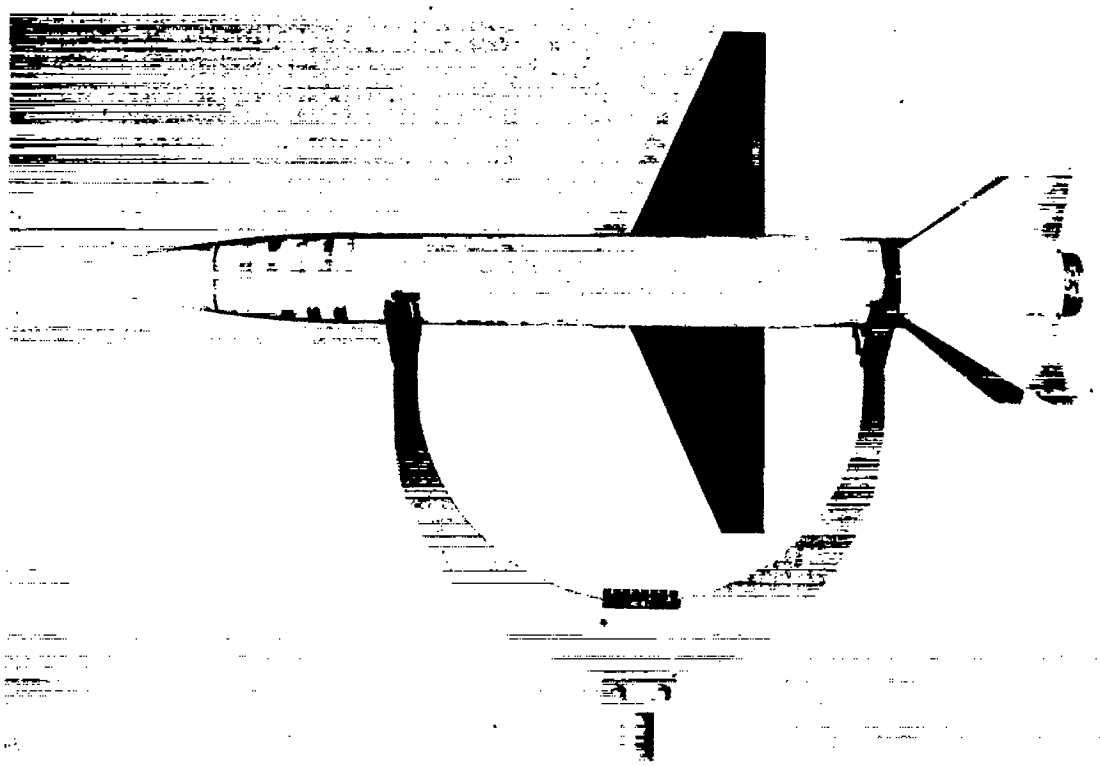

L-64603

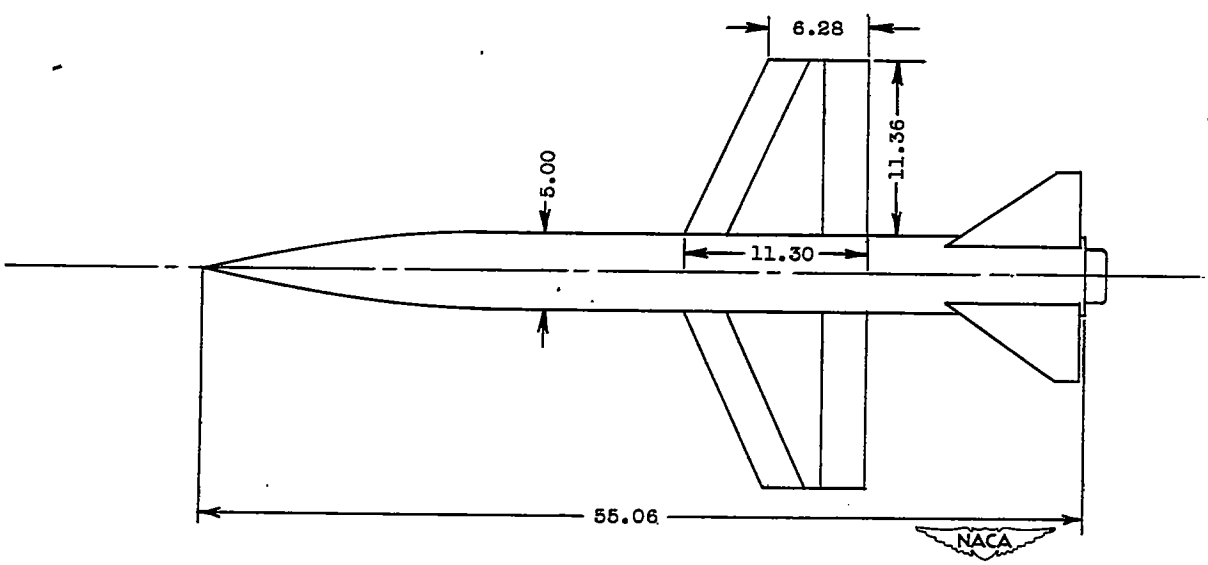

Figure 5.- Model for determining drag of vertical tail. (All dimensions are in inches.)

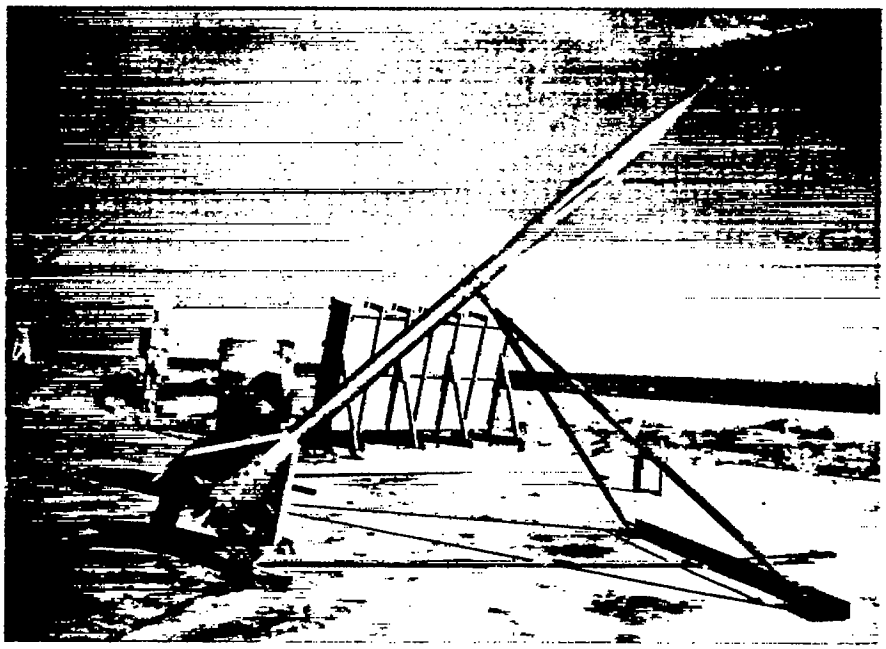

(a) Model A.

NACA
L-59673

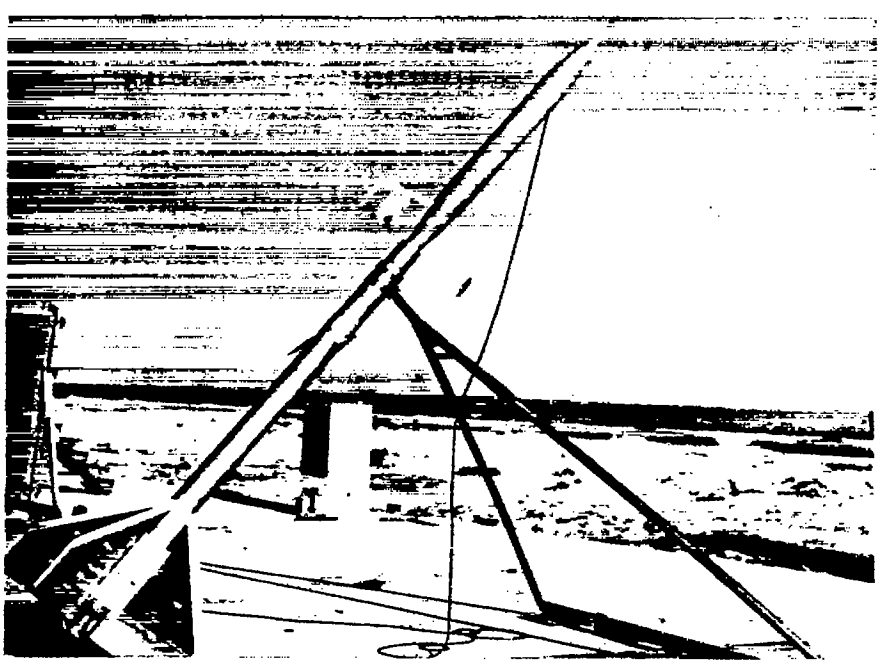

(b) Model C.

NACA
L-63350

Figure 6.- Models on launcher.

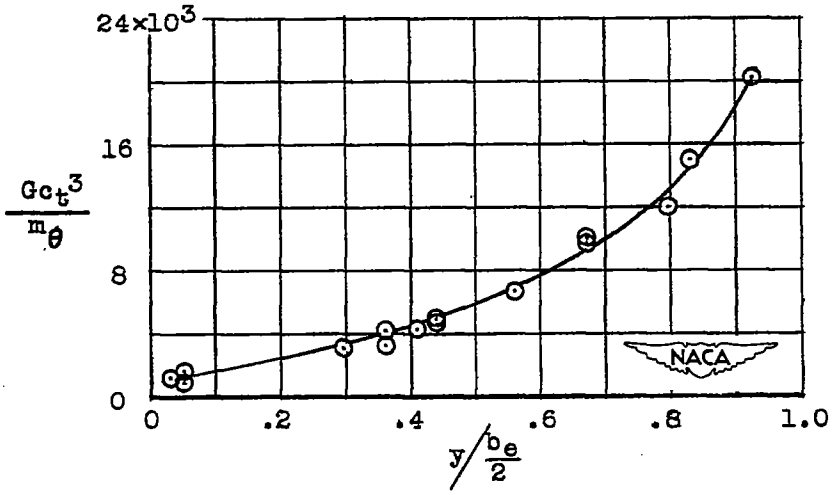

Figure 7.- Measured torsional rigidity of wings.

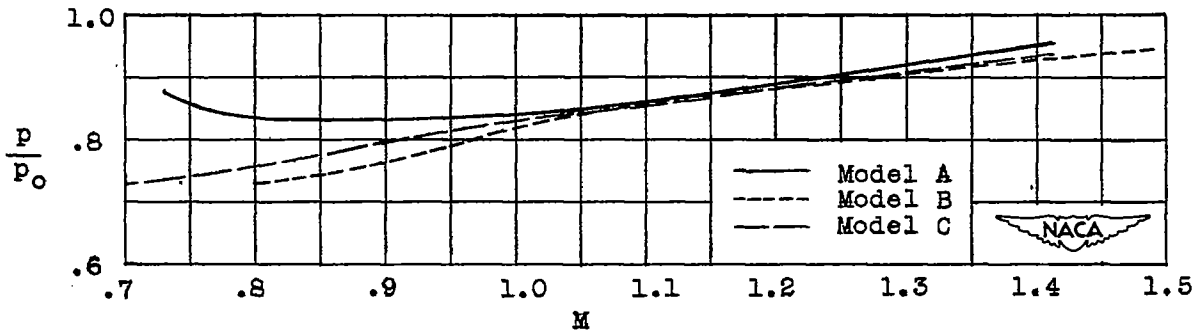

Figure 8.- Static pressure ratio.

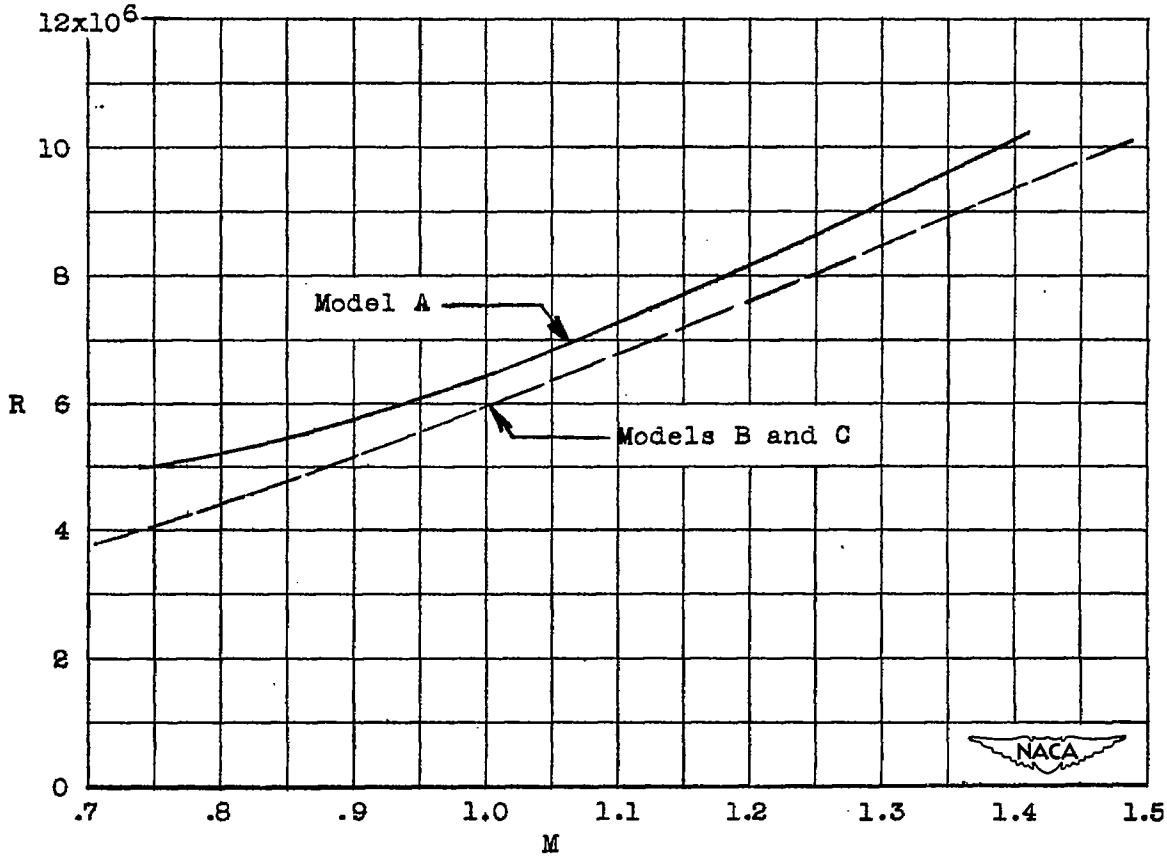

Figure 9.- Reynolds number of tests based on mean aerodynamic chord.

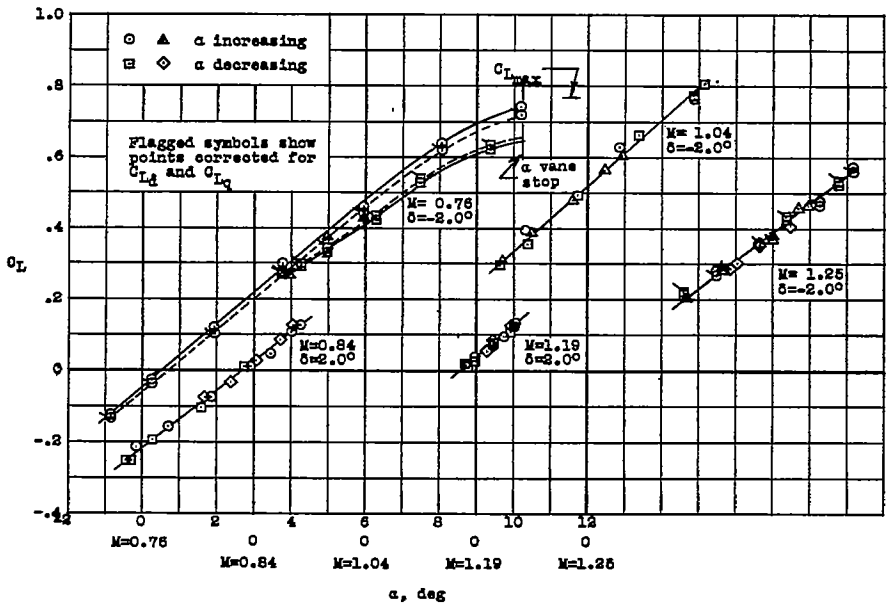

(a) Model A.

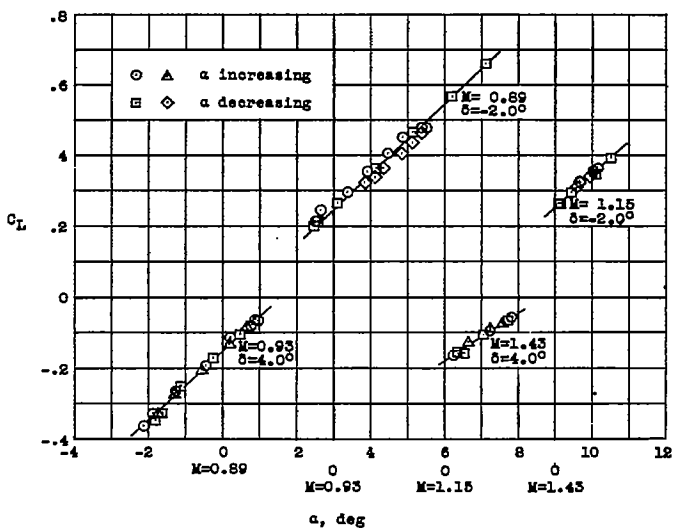

(b) Model B.

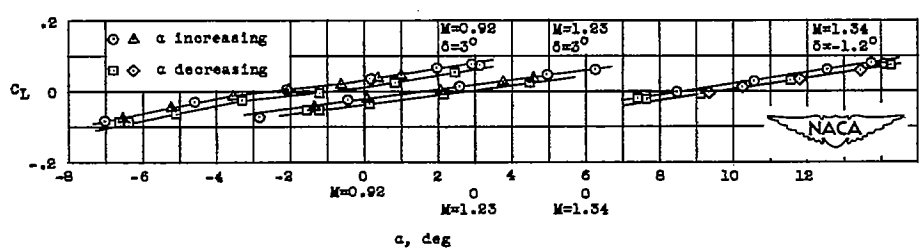

(c) Model C.

Figure 10.- Variation of lift coefficient with angle of attack during several typical oscillations.

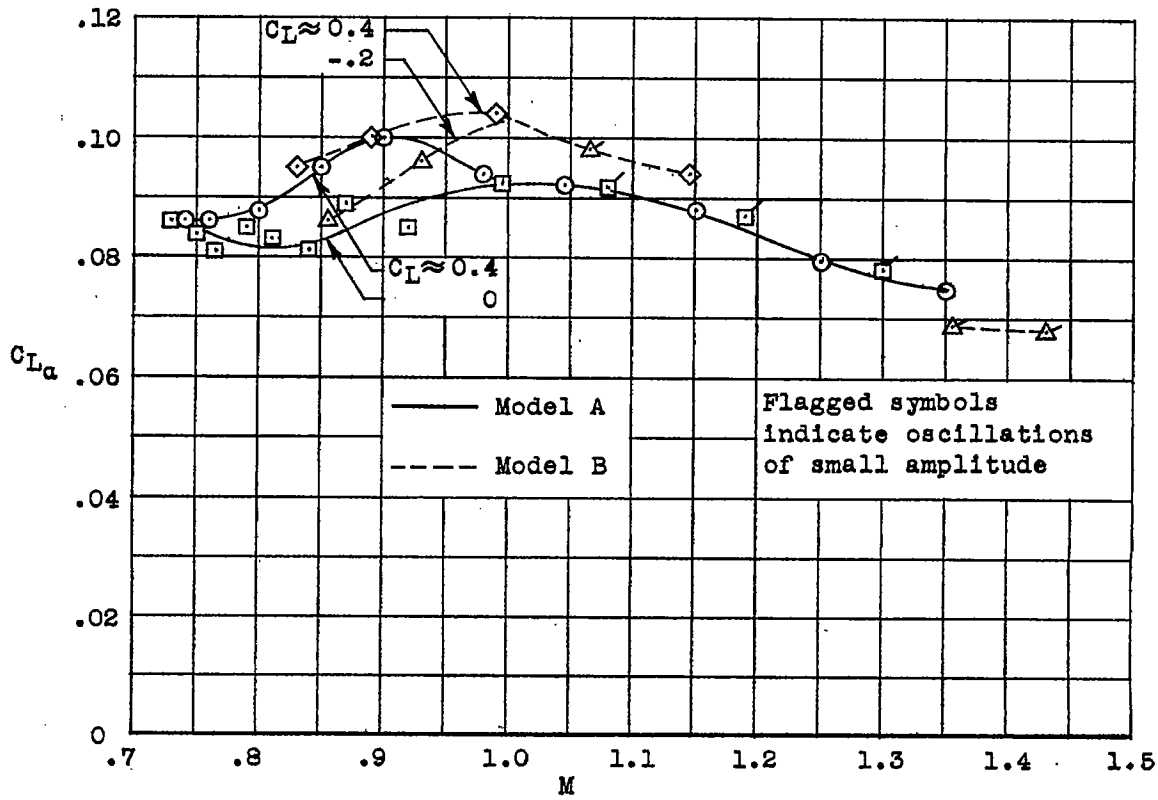

(a) Models A and B.

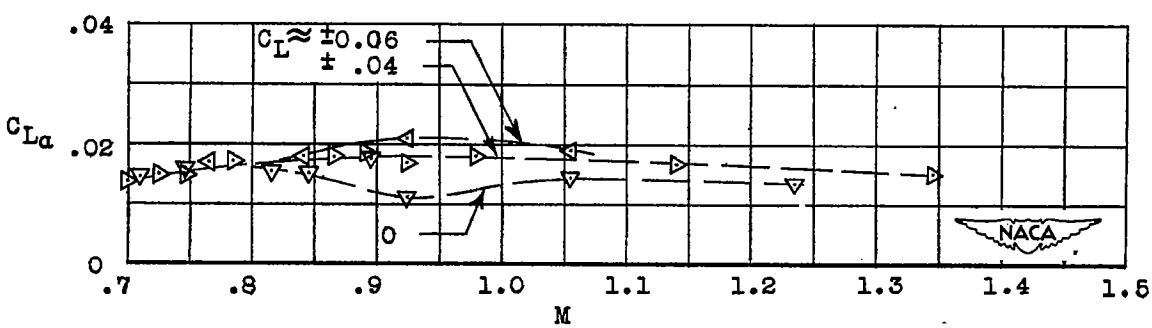

(b) Model C.

Figure 11.- Lift-curve slopes of complete models.

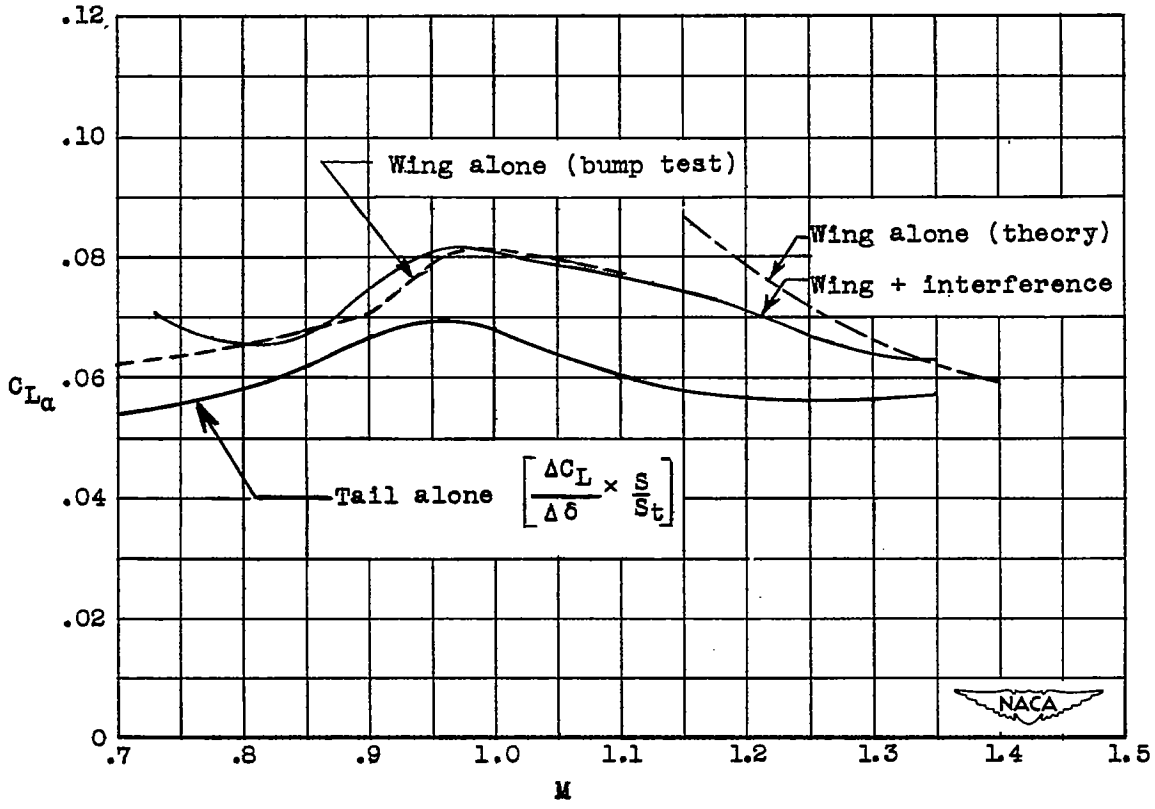

Figure 12.- Lift-curve slopes of wing and tail.

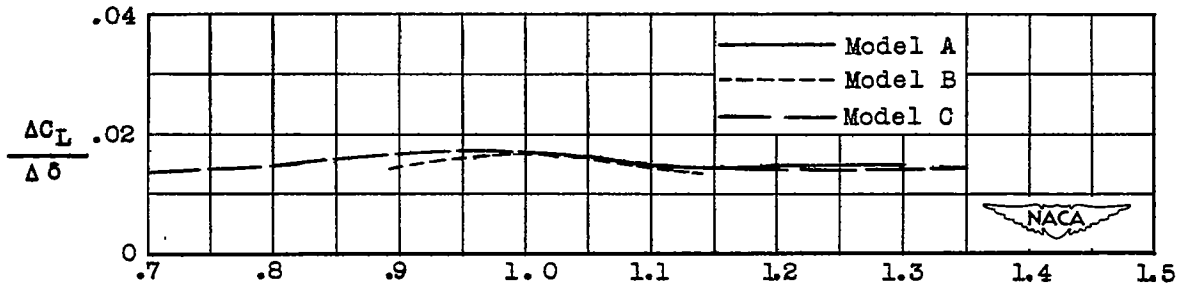

Figure 13.- Lift effectiveness of elevator.

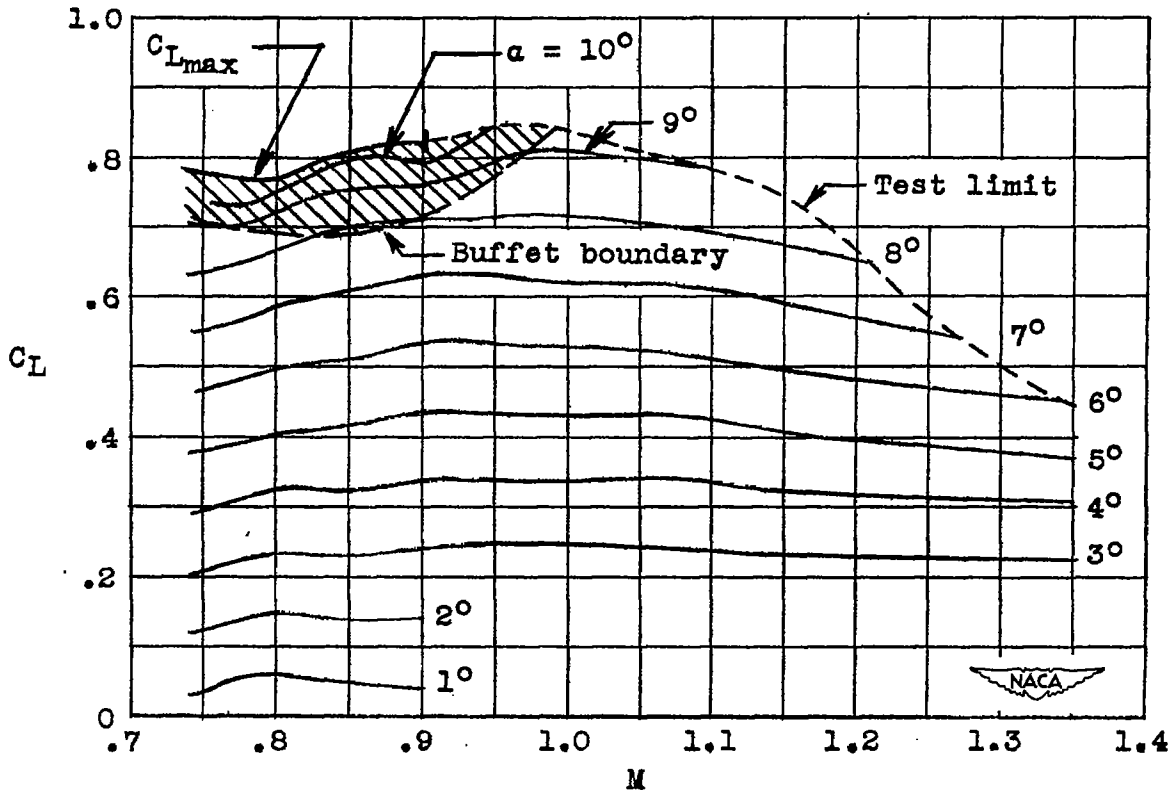

Figure 14.- Summary of buffet and maximum lift information. $\delta = -2.0^{\circ}$.

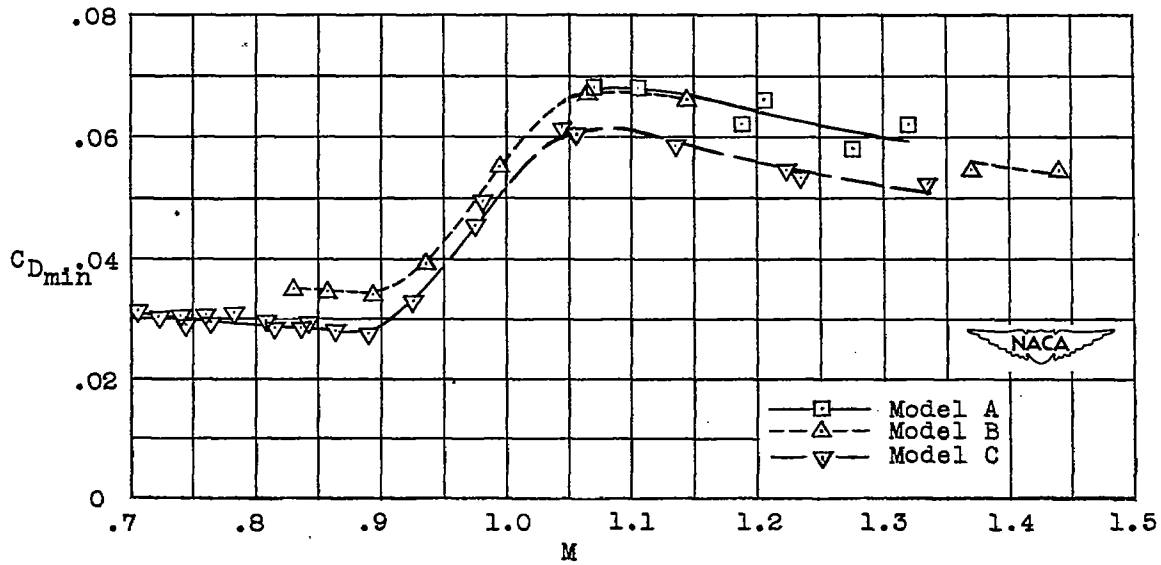

Figure 15.- Minimum drag coefficients of complete models.

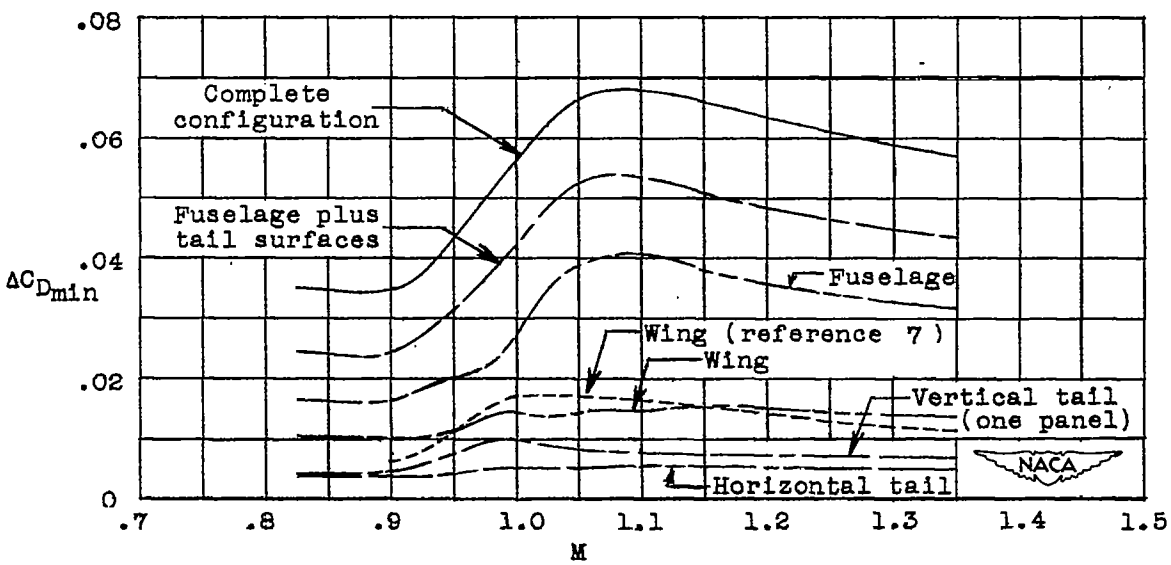

Figure 16.- Minimum drag coefficients of model components.

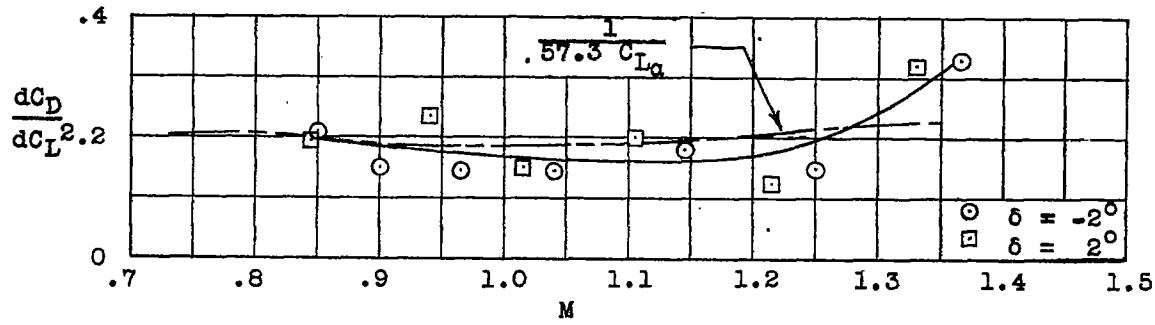

(a) Model A.

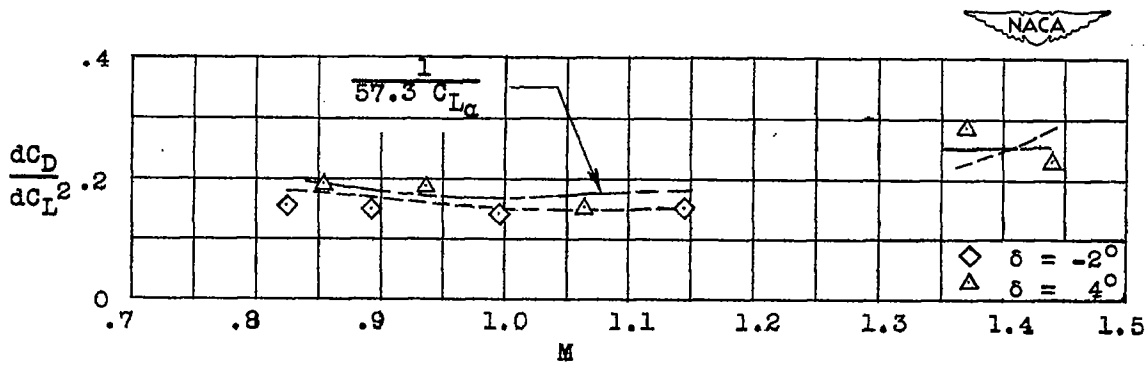

(b) Model B.

Figure 17.- Effect of lift on drag.

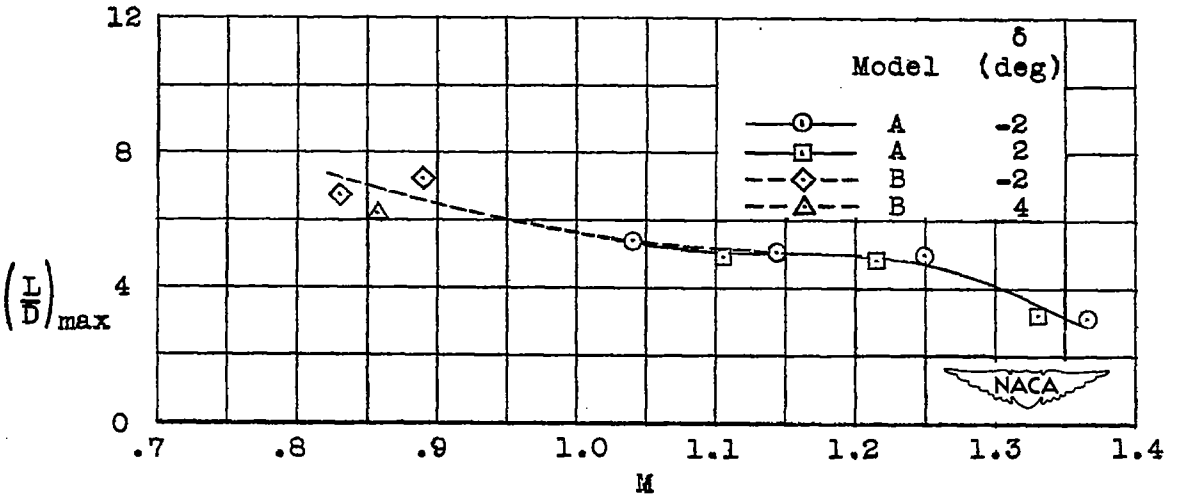

Figure 18.- Maximum lift-drag ratios.

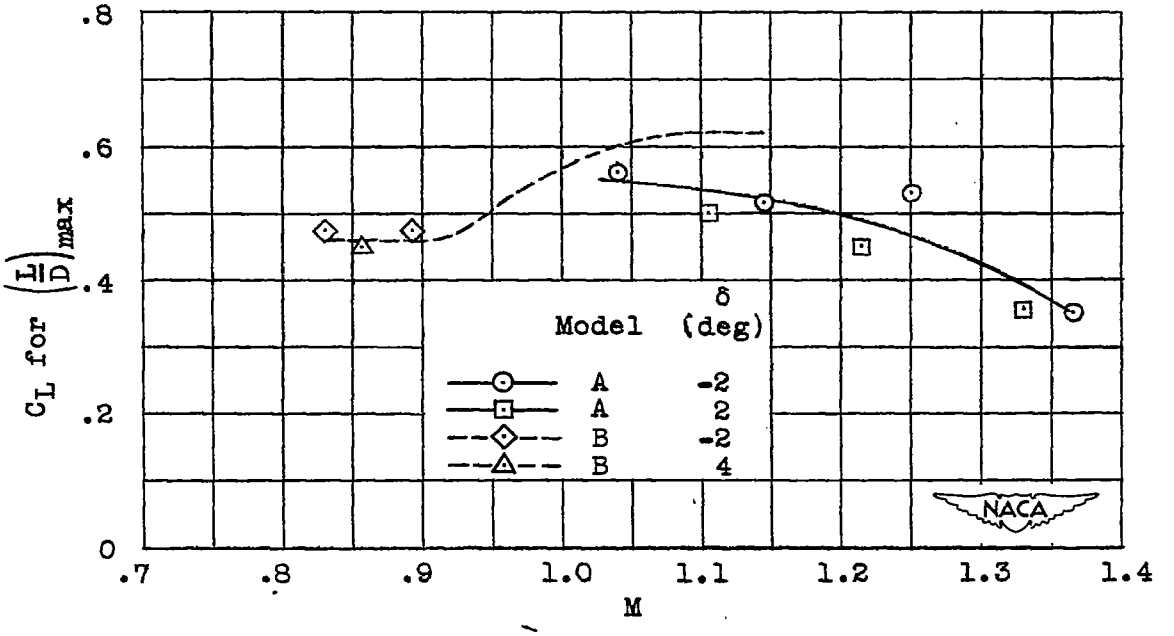

Figure 19.- Lift coefficients at which maximum lift-drag ratios occur.

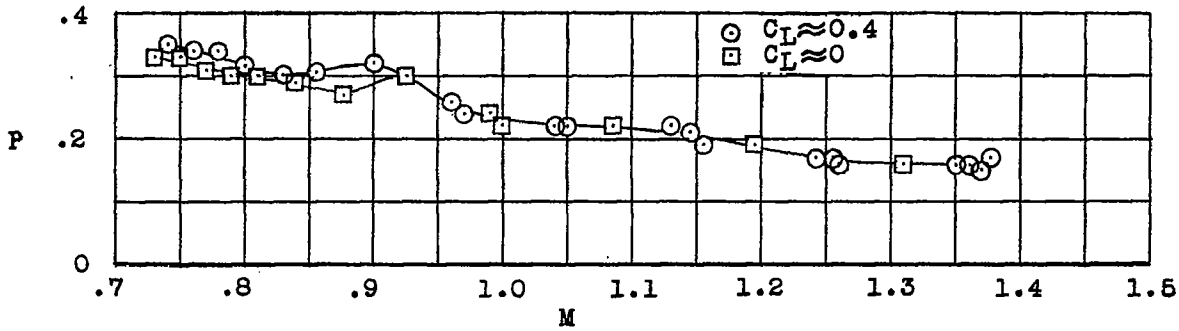

(a) Model A.

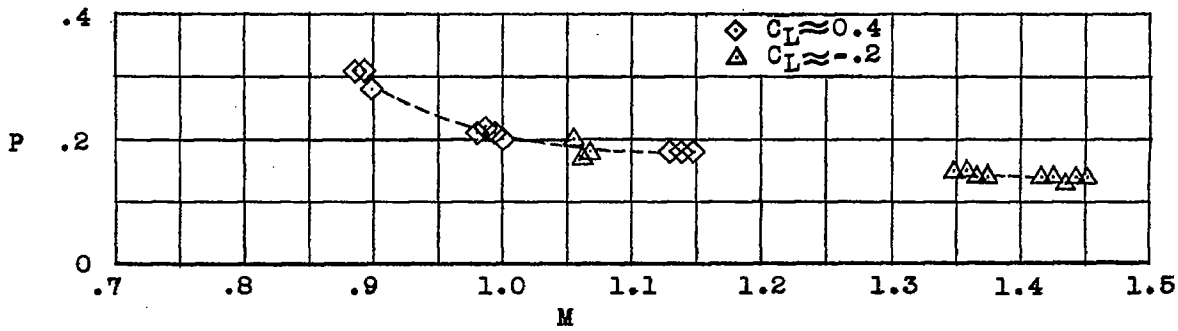

(b) Model B.

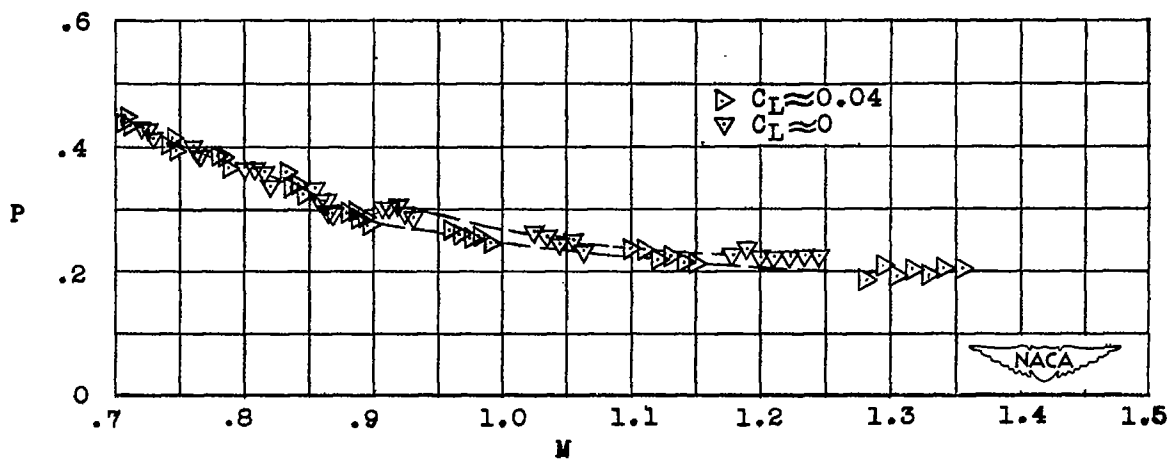

(c) Model C.

Figure 20.- Periods of oscillations.

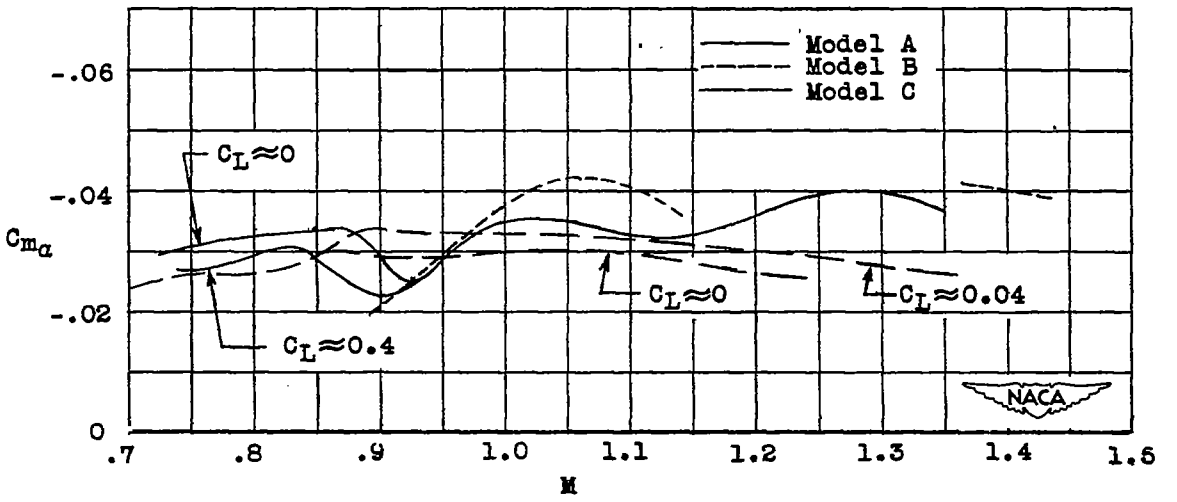

Figure 21.- Static stability of complete models. Center of gravity at 12.4 percent of the mean aerodynamic chord.

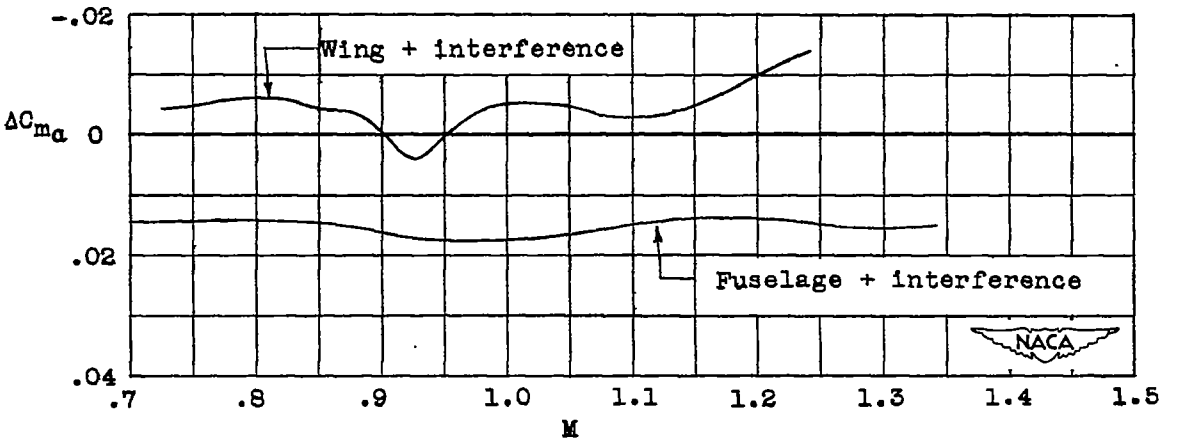

Figure 22.- Static stability increments caused by wing and fuselage. Center of gravity at 12.4 percent of the mean aerodynamic chord.

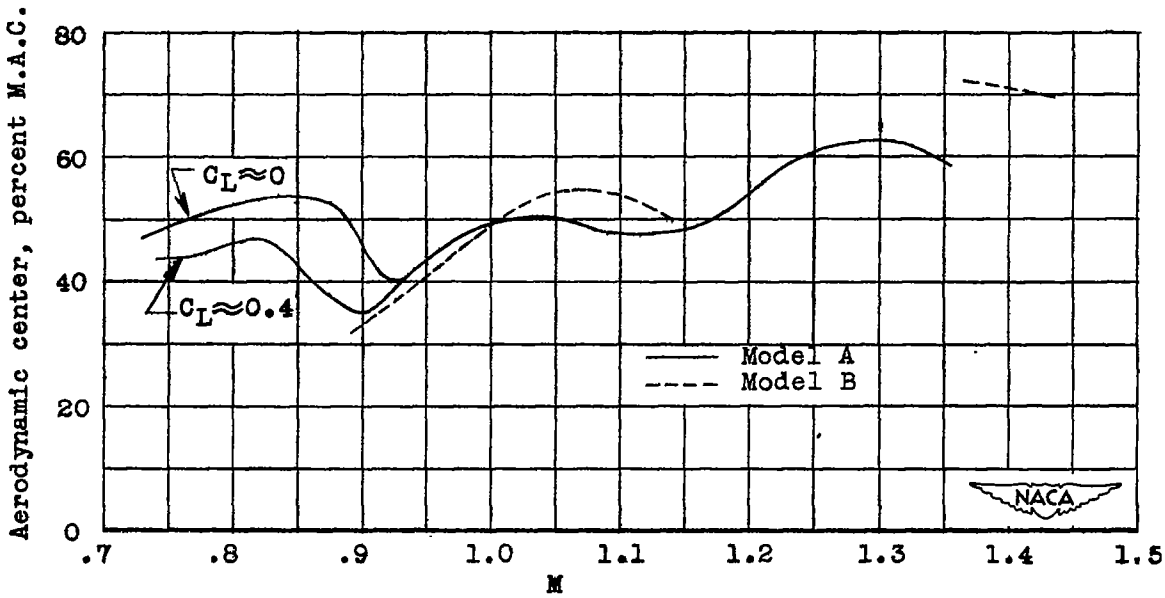

Figure 23.- Aerodynamic-center location.

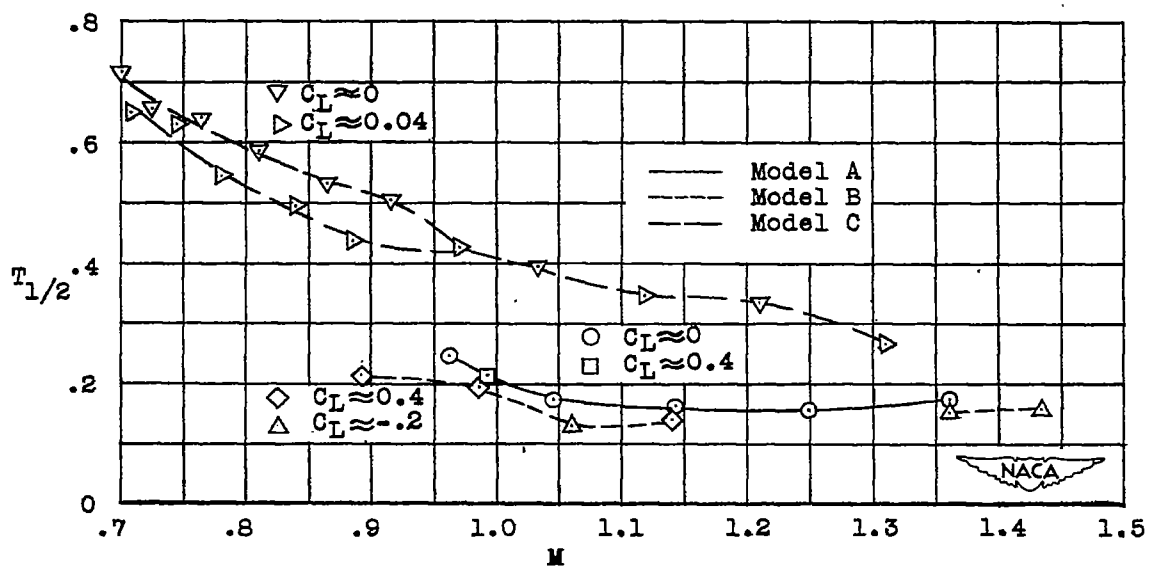

(a) Time to damp to one-half amplitude.

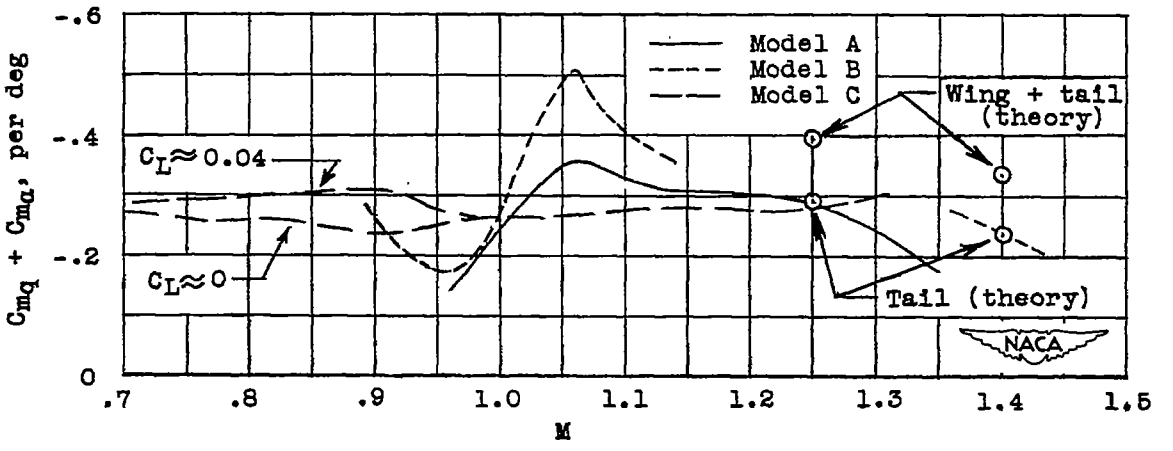

(b) Pitching-moment damping factor $\left(C_{m_q} + C_{m_{\dot{\alpha}}}\right)$.

Figure 24.- Damping characteristics of short-period oscillations.

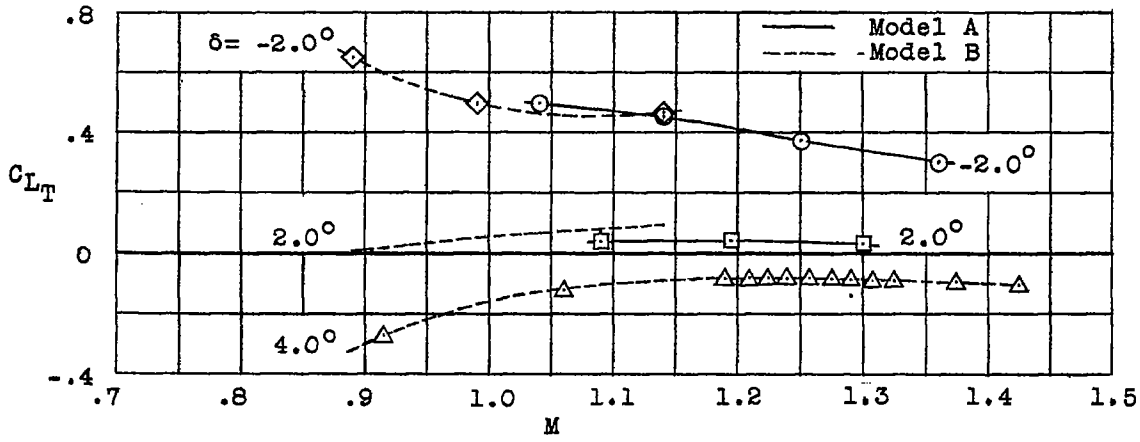

(a) Trim lift coefficients.

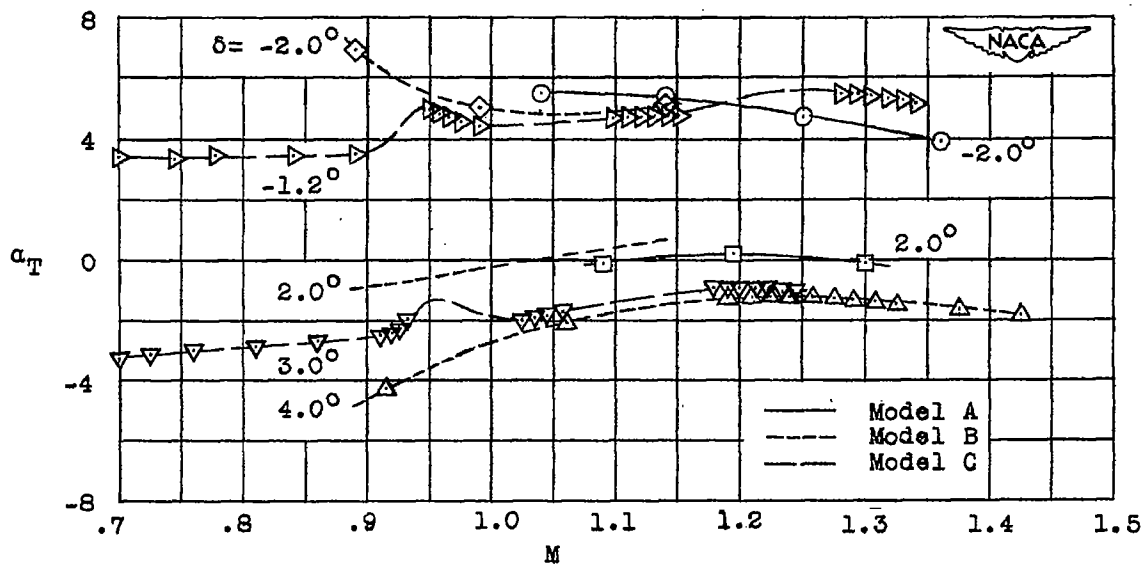

(b) Trim angles of attack.

Figure 25.- Longitudinal trim characteristics.

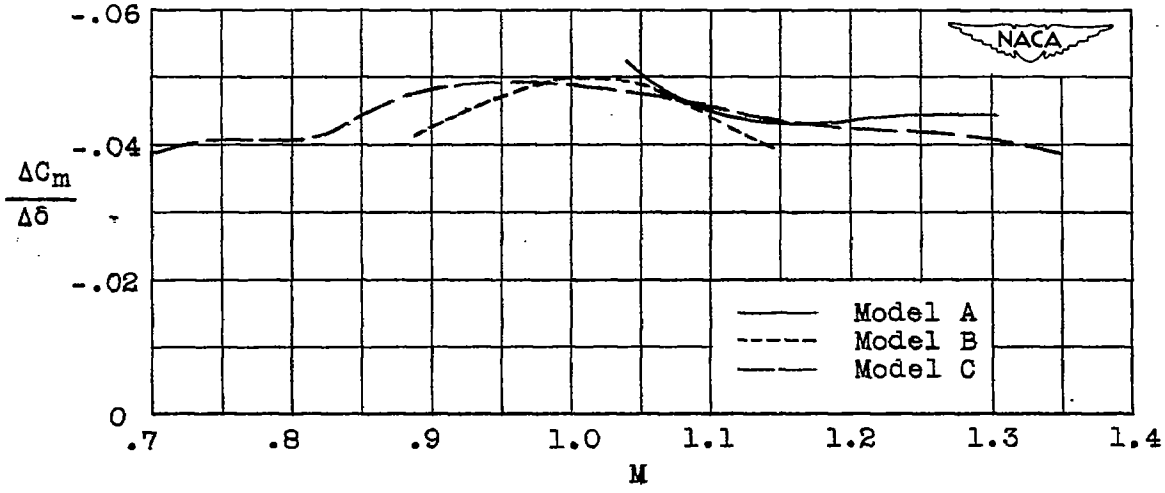

Figure 26.- Effectiveness of the elevator in producing pitching moment.

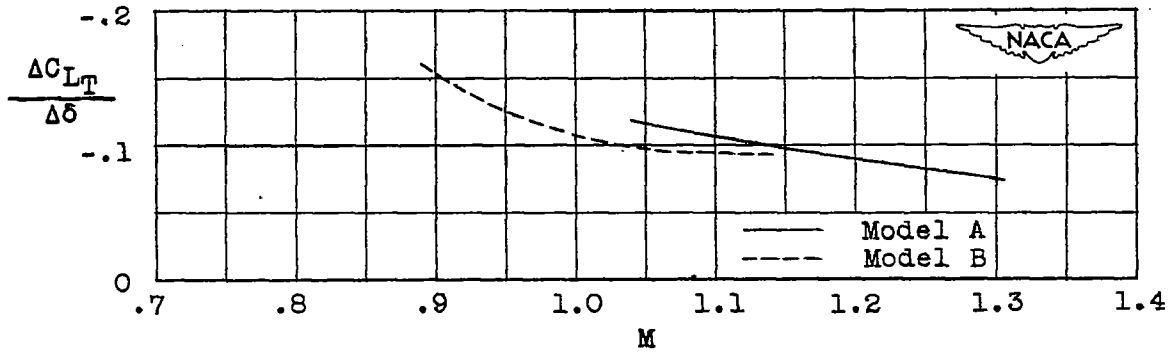

Figure 27.- Change in trim lift coefficient per degree change in elevator deflection.

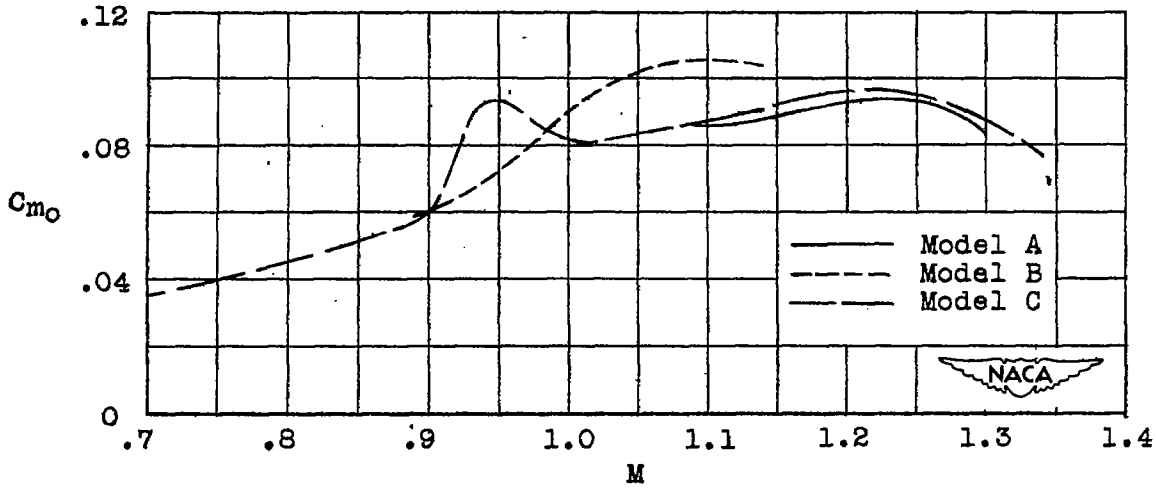

Figure 28.- Pitching-moment coefficient at zero angle of attack and zero elevator deflection.

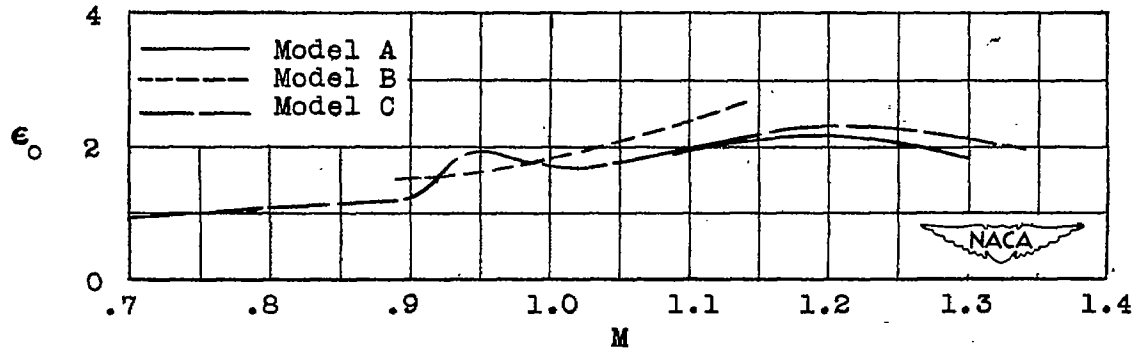

Figure 29.- Downwash angle at zero angle of attack.

NACA-Langley - 3-14-51 - 325